

Electronic Theses and Dissertations, 2004-2019

2010

Thermal Performance Of Cryogenic Multilayer Insulation At Various Layer Spacings

Wesley Louis Johnson
University of Central Florida

 Part of the [Aerospace Engineering Commons](#)
Find similar works at: <https://stars.library.ucf.edu/etd>
University of Central Florida Libraries <http://library.ucf.edu>

This Masters Thesis (Open Access) is brought to you for free and open access by STARS. It has been accepted for inclusion in Electronic Theses and Dissertations, 2004-2019 by an authorized administrator of STARS. For more information, please contact STARS@ucf.edu.

STARS Citation

Johnson, Wesley Louis, "Thermal Performance Of Cryogenic Multilayer Insulation At Various Layer Spacings" (2010). *Electronic Theses and Dissertations, 2004-2019*. 1622.
<https://stars.library.ucf.edu/etd/1622>

THERMAL PERFORMANCE OF CRYOGENIC MULTILAYER INSULATION AT
VARIOUS LAYER SPACINGS

by

WESLEY LOUIS JOHNSON
B.A.E. Auburn University, 2007

A thesis submitted in partial fulfillment of the requirements
for the degree of Master of Science in Aerospace Engineering
in the Department of Mechanical, Materials, and Aerospace Engineering
in the College of Engineering and Computer Science
at the University of Central Florida
Orlando, Florida

Fall Term 2010

The following is the result of research completed as a portion of the author's duties as an employee of the National Aeronautics and Space Administration. This work is hereby declared a work of the government and not subject to copyright within the United States of America.

ABSTRACT

Multilayer insulation (MLI) has been shown to be the best performing cryogenic insulation system at high vacuum (less than 10^{-3} torr), and is widely used on spaceflight vehicles. Over the past 50 years, many numerous investigations of MLI have yielded a general understanding of the many variables associated with MLI. MLI has been shown to be a function of variables such as warm boundary temperature, the number of reflector layers, and the spacer material in between reflectors, the interstitial gas pressure and the interstitial gas. Because conduction between reflectors increases with the thickness of the spacer material, and yet the radiation heat transfer is inversely proportional to the number of layers, it stands to reason that the thermal performance of MLI is a function of the number of layers per thickness, or layer density. Empirical equations that were derived based on some of the early tests showed that the conduction term was proportional to the layer density to a power. This power depended on the material combination and was determined by empirical test data.

Many authors have graphically shown such optimal layer density, but none have provided any data at such low densities, or any method of determining this density. Keller, Cunnington, and Glassford showed MLI thermal performance as a function of layer density of high layer densities, but they didn't show a minimal layer density or any data below the supposed optimal layer density. However, it was recently discovered by the author that by manipulating the derived empirical equations and taking a derivative with respect to layer density, a solution for on optimal layer density may be obtained.

Several manufacturers have begun manufacturing MLI at densities below the analytical optimal density. This trend is apparently based on the theory that increased distance between layers lowers the conductive heat transfer and that there are no limitations on volume. By modifying the circumference of these blankets, the layer density can easily be varied. The most direct method of determining the thermal performance of MLI at cryogenic temperature is by evaporation (or “boil-off”) calorimetry. Several blankets were procured and tested at various layer densities by the Cryogenics Test Laboratory at NASA Kennedy Space Center. The blankets were tested over a wide range of layer densities including the analytical minimum. Several of the blankets were tested at the same insulation thickness while changing the layer density (thus a different number of reflector layers).

Heat transfer optimization of the layer density of multilayer insulation systems would remove the variable of layer density from the complex method of designing such insulation systems. Since the layer density is one of the variables that in those complex equations that require more experience to understand fully grasp, this significantly simplifies the blanket design process. Additional testing was performed at various warm boundary temperatures and pressures. The testing and analysis was performed to determine thermal performance data and to simplify the analysis of cryogenic thermal insulation systems.

ACKNOWLEDGMENTS

I would like to acknowledge that the funding for this study was provided by the Exploration Technology Development Program, Cryogenic Fluid Management Project. This study contributed to two project tasks: Methane Lunar Surface Thermal Control (MLSTC) and Multilayer Insulation Fabrication and Multilayer Insulation Uncertainty Experiment.

I would like to acknowledge Mr. James Fesmire for his help in planning and performing the testing described in this report. Without his knowledge and expertise in cryogenic testing of thermal insulation systems along with his willingness to openly share the tiny and most important details, this work would never have occurred. I also acknowledge Mr. Wayne Heckle for his expert help and dedication in the testing. Much of my understanding of testing comes from these two men who have been performing similar tests for many years.

Dr. Glen McIntosh, Mr. Steve Sutherlin, and Mr. Eric Hyde have pushed me in the understanding of heat transfer in multilayer insulation and have freely shared their knowledge on the subject to point me in the proper directions to make this work a reality.

Mr. Alan Kopelove, Mr. Scott Dye, and Quest Product Development permitted me to publish the results from testing their insulation system produced as part of a recent SBIR project.

TABLE OF CONTENTS

LIST OF FIGURES	viii
LIST OF TABLES	x
LIST OF ACRONYMS	xi
LIST OF NOMENCLATURE	xiii
CHAPTER ONE: INTRODUCTION.....	1
CHAPTER TWO: BACKGROUND & LITERATURE REVIEW	6
Multilayer Insulation.....	6
Calorimeters.....	9
CHAPTER THREE: THEORY	17
MLI Heat Transfer	17
Layer Density Optimization.....	22
CHAPTER FOUR: TEST METHODOLOGY	27
Experimental Setup.....	27
Experimental Measurement, Uncertainty, and Variability	33
Insulation Specimens	37
CHAPTER FOUR: RESULTS AND DISCUSSION	42
Test Results.....	43
Discussion.....	49
Performance at High Vacuum.....	50
Performance at Degraded and No Vacuum.....	56

Modification of McIntosh Model for all Pressure Regimes	58
CHAPTER FIVE: CONCLUSIONS	63
APPENDIX: VARIOUS DATA PLOTS FROM TESTING	65
REFERENCES	79

LIST OF FIGURES

Figure 1: Ames Research Center Calorimeter (Courtesy of NASA) [31]	12
Figure 2: Lockheed guarded flat-plate electrical calorimeter (Courtesy NASA and Lockheed) [17].....	13
Figure 3: GRC calorimeter (Figure 3 from reference [36]), Courtesy NASA Glenn Research Center	16
Figure 4: Heat flux as a function of layer density with a constant number of layers [1, 2, 11, 16, 17, 45]	19
Figure 5: Heat Flux as a function of layer density for a constant thickness (25.4 mm) [1, 2, 11, 16, 17, 45]	20
Figure 6: Heat Flux, Thermal Conductivity, and Estimated Mass for MLI as a function of Layer Density with 40 shields [1, 17]	22
Figure 7: Optimal Layer Densities for Perforated Double Aluminized Mylar and Dacron Net MLI configurations as a function of boundary temperatures for $P = 10^{-5}$ Torr [17, 45]	26
Figure 8: Absolute Cylindrical Boil-off Calorimetry	27
Figure 9: Error Calculation for Stratified Cryostat-100.....	30
Figure 10: Cryostat-100 backpressure control system for dampening the effect of the atmospheric tides on the boil-off cryogen.	36
Figure 11: Comparison of Flow Variation before and After Installation of Back Pressure Control System.....	37
Figure 12: Typical Velcro attachment for MLI Coupon A.....	38

Figure 13: Typical tape attachment on MLI Coupon B using a small piece of Dacron netting to minimize thermal bridging.....	39
Figure 14: IMLI plastic spacer grid	40
Figure 15: IMLI Cryostat-100 layup.....	41
Figure 16: Heat flux as a function of CVP for various MLI systems as a WBT of 305 K.....	46
Figure 17: Effective thermal conductivity (k-value) as a function of CVP for MLI systems at a WBT of 305 K	47
Figure 18: High vacuum heat flux for various MLI systems.....	48
Figure 19: High vacuum effective thermal conductivity (k-value) for various MLI systems	48
Figure 20: No vacuum k-value test results for various MLI system testing	49
Figure 21: Test data as function of layer density	55
Figure 22: Thermal conductivity test data plotted as a function of layer density.....	56
Figure 23: Temperature profiles for test series A138.	58
Figure 24: Heat Flux vs CVP for several MLI systems.....	59
Figure 25: Heat Flux as a Function of Inverse Knudsen Number for Several MLI Systems	62

LIST OF TABLES

Table 1: Geometric properties of the 12th layer of A125	32
Table 2: Measured conduction heat load for all vacuum pressures	32
Table 3: Thermocouple placement for each test series	33
Table 4: Key Geometrical Parameters for MLSTC Cryostat-100 Testing	42
Table 5: Test results for calorimeter testing (Part I)	43
Table 6: Test results for calorimeter testing (Part II)	45
Table 7: Correlation Comparisons to Test Results	51
Table 8: Power Factors of and Optimal Layer Densities Various MLI Equations	53
Table 9: Effect of Layer Density on Heat Flux and Mass	54

LIST OF ACRONYMNS

AFAL	Air Force Astronautics Laboratory (does not currently exist)
BATC	Ball Aerospace & Technology Corporation
CBT	Cold Boundary Temperature
CFM	Cryogenic Fluid Management
CTL	Cryogenics Test Laboratory
CVP	Cold Vacuum Pressure
DAM	Double Aluminized Mylar
ETDP	Exploration Technology Development Program
GRC	John Glenn Research Center (Cleveland, OH)
IIT	Indian Institute of Technology
IMLI	Integrated Multilayer Insulation
KSC	John F. Kennedy Space Center (Kennedy Space Center, FL)
LE	Lockheed Equation
LEO	Low Earth Orbit
LSF	Lockheed Scale Factor
MHTB	Multi-purpose Hydrogen Testbed
MLE	Modified Lockheed Equation
MLI	Multilayer Insulation
MLSTC	Methane Lunar Surface Thermal Control Task
MSFC	George C. Marshall Space Flight Center (Huntsville, AL)

NASA	National Aeronautics and Space Administration
PID	Proportional, Integral, and Derivative controls
RTD	Resistance Temperature Detector
SBIR	Small Business Innovative Research
SCCM	Standard Cubic Centimeters per Minute (1/1000 standard liters per minute)
SMiRF	Small Multipurpose Research Facility
WBT	Warm Boundary Temperature

LIST OF NOMENCLATURE

A	Area, m ²
A _m	Mean area of heat transfer, m ²
C _G	Coefficient of gaseous conduction heat transfer (empirical)
c _p	Specific heat at constant pressure, kJ/kg
C _R	Coefficient of radiation heat transfer (empirical)
C _S	Coefficient of solid conduction heat transfer (empirical)
c _v	Specific heat at constant volume, kJ/kg
D _i	Inner diameter of cylindrical insulation, m
D _o	Outer diameter of cylindrical insulation, m
h	Conductivity per unit area or convection coefficient, W/m ² -K
H	Energy transfer per unit time per unit surface area, W/m ²
k	Apparent thermal conductivity, mW/m-K
k _B	Boltzman's constant, 2.33*10 ⁻²⁰ (need units)
Kn	Knudsen number (λ/x)
L	Length of cylinder, m
M	Molecular weight (nitrogen = 28.014), g/mol
N	Number of layers
\bar{N}	Layer density, layer/cm
P	Pressure, torr
PF	Power Factor, exponential relationship between two parameters

q''	Heat flux, W/m^2
Q	Power, W
R	Universal gas constant, $8.314 J/K\text{-mol}$
T	Temperature, K
T_c	Cold Boundary Temperature, K
T_h	Warm Boundary Temperature, K
ΔT	Temperature difference, K
Δx	Insulation thickness perpendicular to area of heat transfer, m
α	Accommodation coefficient
γ	ratio of specific heats, (c_p/c_v)
ϵ	Total hemispherical emissivity
λ	Mean Free Path, m
ξ	Diameter of a gas molecule, m (for nitrogen $3.14 * 10^{-10} m$)
π	Irrational number defined as the ratio of the circumference to the radius of a circle
σ	Stephan-Boltzmann constant, $5.67*10^{-8} W/m^2\text{-K}^4$

CHAPTER ONE: INTRODUCTION

Heat transfer is at the heart of life on earth as we know it. Radiation from the sun beams down on earth after travelling 93 million miles from the surface of the sun to the surface of the earth keeping the earth in a habitable condition. Convection and conduction from water boiling over a hot bed of coals or fire are at the heart of many of the power plants that dot the country and provide the power that runs modern society. Alternatively, the removal of heat is just as important in the operation of air conditioners that keep many homes and offices cool as well as in refrigerators and freezers that preserve food for long durations. Yet at the heart of heat transfer is insulation. While many operations depend on the transfer of thermal energy, they depend just as much on the containment of that same thermal energy. The earth contains an atmosphere that traps radiation and other forms of heat to minimize the night time cooling of the earth and keep the temperature band generally within 30 degrees Celsius. However, on celestial bodies without such atmospheres, such as our moon, the temperature can swing in excess of 250 degrees Celsius between day and night. Similarly, in modern power plants, the efficiency of the power plant is what makes a successful power plant. This efficiency is determined by the plants ability to contain the energy it produces and minimize the heat transfer that is lost to its surroundings. Thus the efficiency of insulation plays a large role in energy usage, efficiency, and the advancement of society.

There are three general forms of heat transfer: radiation, conduction, and convection. Radiation is caused by the transfer of photons through a space. It does not require a media

through which to travel, and is prevented by reflecting the photons. Surfaces have properties, often called optical properties, that determine the propensity of the surface to emit (or generate or reflect, as in a source) photons, to absorb (as in a sink) photons, or to transmit photons (allow them to pass through). These properties are known respectively as emissivity, absorptivity, and transmissivity, and are on a scale from zero to one, representing the percentage of photons acting in each case. Because heat transfer is related to the reaction of these photons between surfaces, radiation can be generically represented as follows:

$$q'' = \sigma \epsilon (T_h^4 - T_c^4) \quad (1)$$

Conduction is the transfer of energy through a media, usually in reference to a solid material, but also in reference to a gaseous or liquid material. Conduction is also based on material properties, in general the ease of energy transfer through the material is known as conductivity, or thermal conductivity. Additionally, the material has a certain quantity of energy that raises the temperature of the material. This property is known as the specific heat of the material. Thus the relationship between the conductivity and the specific heat can be arranged to determine how quickly the energy will be dispersed through the material (i.e. how quickly can the conductivity get the energy to remote parts of the material while the energy is absorbed along the way in heating the material). This property is known as thermal diffusivity. Conduction heat transfer is generally considered using the Fourier equation:

$$q'' = -k \frac{\partial T}{\partial x} \quad (2)$$

However, because heat transfer is a function of the temperature difference and not of exact temperature, the Fourier expression can be expressed more appropriately as:

$$Q = - \int \frac{A}{\partial x} \int_{T_c}^{T_h} k \partial T \quad (3)$$

Where the first integral is the shape factor and the second integral is the apparent thermal conductivity integral at the given temperature difference. The thermal conductivity of a material is determined by experimental means.

Convection is type of conduction through a moving media, such as a flowing liquid or gas. Because the flowing motion of the media allows for a quicker dispersion of the energy, convection generally transfers more energy than conduction through the same media would. Convection heat transfer is determined experimentally and published as a convection coefficient, h that fits the form of:

$$q'' = h(T_h - T_c) \quad (4)$$

There has been much effort put forth to determine the best methods of minimization of heat transfer. At ambient temperatures, both convection and conduction when present tend to be much more important than radiation as the energy flow through these paths is much greater than through radiation alone. Thus any method of eliminating any form of heat transfer by these methods is highly sought after.

A simple method to eliminate or minimize convection and gaseous conduction is to simply remove the gas. This is done by pulling a vacuum on the insulation in question. Now, within the vacuum we only have any solid conduction and radiation to deal with. Conduction can be dealt with by simply increasing the vacuum space between the hot side and cold side using minimal structural supports to keep them at a distance. The radiation can be greatly

minimized by putting reflective shields in between the hot side and cold side. This effectively divides the heat transfer by the number of shields (N) that are used such that:

$$q'' = \frac{\sigma \epsilon (T_h^4 - T_c^4)}{N} \quad (5)$$

Thus by putting many reflective shields in between the hot side and cold side, the heat transfer is greatly reduced. This works very effectively as long as my reflective shields don't touch each other or anything else for that matter, they must effectively become floating shields [1]. Anything physically put in between these shields to hold them apart, keep them from touching each other, or keep them from touching either boundary degrades the value of the insulation by introducing conduction between these layers. This conduction will always degrade the insulation system performance [2]. Multilayer insulation systems are built upon this trade, many radiation layers reduces the radiation heat transfer; however the conduction between layers must be kept to a minimum.

These principles are important in the design of thermal insulation systems for many terrestrial applications where the isolation of the warm and cold boundaries contributes greatly to the efficiency of the application. Cryogenic applications are one of the many types of systems where this principle is very much in play. Cryogenic systems are usually several hundred degrees below the earth's ambient temperature, and thus the temperature differences across the insulation systems can be as large as several hundred degrees Celsius. Thus the building and maintenance of vacuum jacketed insulation systems is a must for system efficiency and the long term profitability of cryogenic procedures. These principles are even more important outside of the Earth's protective atmosphere, while the vacuum is provided there, the efficiency of the

reflection shields is much more important due to the large amounts of radiation heat transfer from both the sun and the earth (or other celestial bodies that may be in a closer proximity to that particular spacecraft).

Recently, NASA has become interested in long duration storage of cryogenic propellants such as oxygen, hydrogen, and methane in Low Earth Orbit (LEO) and beyond. Thus high performance MLI once again has become very important in the design and fabrication of new spacecraft. A complete understanding of MLI needs to be established, including all variables that come into play when designing and fabricating these systems. While system level demonstrations of passive thermal insulation systems (no cryocoolers or other active cooling mechanisms) can show that an engineering knowledge of MLI exists presently as long as enough conservatism is used, some of the more precise (and hard to measure) variables are not as well understood and accounted for. This has led to a recent activity, the Methane Lunar Surface Control Test (MLSTC), to request calorimeter testing of their MLI system, in order to aid in the design and development of future systems, two different MLI systems were bought, the first was designed exactly and the insulation system was designed for the system level test and the second to allow for the change of a key and largely quantified variable, the layer density. Thus the second blanket system was designed such that it could be installed on the cylindrical calorimeter in successively tighter configurations by removing portions of the blanket and reinstalling. The importance for this testing for the MLSTC is that comparing the calorimeter results with the system level test results and taking into account the structural support system for the tank, effects of these structural penetrations can be determined.

CHAPTER TWO: BACKGROUND & LITERATURE REVIEW

Calorimeters and MLI have often been joined together in development projects. In order to understand the small idiosyncrasies of the heat transfer through MLI, high performance calorimeters are needed. These calorimeters must measure thermal performance on the order of milliwatts or even microwatts to be able to detect the small differences between various MLI systems.

Multilayer Insulation

Multilayered insulation (MLI) was first experimentally tested by Sir James Dewar in 1900 when he experimented with three layers of aluminum foil [3]. However, it was not until the late 1940s when Cornell described his layered radiation shield system that MLI was born [4]. However, Peterson is often credited as the first to describe modern MLI.

With the advent of space travel within the natural vacuum of space and the large quantities of hydrogen needed for the hydrogen bomb, MLI became a highly studied topic with funding from NASA and the Defense Departments. Glaser, Fredrickson, Leonard, and many others continued to research MLI from the 1960s and 1970s, with an underlying premise for applications involving long duration lunar and Martian missions. Glaser, Black, and Hinckley at the A.D. Little Corporation (an offshoot of the Massachusetts Institute of Technology) pushed the theoretical threshold of radiation heat transfer through parallel radiation shields, determination of emissivity of various materials, comparing various seam and penetration concepts, and measuring the effects of compression in MLI systems [5-8]. They also formulated

the physical concepts of which to base future cryogenic stages and long duration hydrogen storage [9, 10].

Fredrickson lead a group of engineers at Douglas Aircraft who sought the optimal design for insulating the Mars Nuclear Vehicle that was being designed by NASA as a follow on program to the Apollo program [11]. Their efforts culminated in the insulation of a 105 inch diameter tank at MSFC and a battery of tests that checked the performance of the insulation at many different environments that were expected to be encountered, from ascent to long duration storage [12]. Eventually, their insulation system did fly on the forward dome of Skylab. During the 2 year Skylab program, no degradation was noted through the insulation, however, the “cold” boundary was the ambient interior of the manned cabin as opposed to the intended liquid hydrogen tank [13].

Leonard and Walburn with their group at General Dynamics/Convair developed novel insulation systems such as Superfloc spacer based MLI, which were micro-needle Dacron tufts that focused on minimizing the conduction area between radiation shields while maximizing contact resistance [14]. They also developed a reusable system that could survive as many as 100 launches on the Space Shuttle Transportation System using a purge and repressurization scheme to minimize the air intrusion and variable pressures that would be seen over the life of the system [15]. Over the course of the 100 pressure cycles, the MLI degraded by 26% between cycles 1 and 52 and 10% between cycles 53 and 100. The post test inspection determined that this effect was due to the opening up of the blankets at the seams during the pressure transients. This work was the first of many research projects in support of the Centaur G-prime project to

put liquid oxygen and liquid hydrogen fueled upper stages in the Shuttle payload bay for delivering satellites to various orbits. Such research and development often focused on trying to define the best system for a specific mission.

In the late 1960s and early 1970s, Brogan, Keller, and Cunnington at Lockheed delivered the most extensive set of data currently in existence on a wide variety of MLI systems [16, 17]. Their tests were completed on both flat plate calorimeters and small tanks. Additionally, the expertise and data from Lockheed were used as the basis for the international standard practice for MLI, ASTM C-740 [18]. Cunnington also worked with Prof. Tien at UCLA on several projects aimed at understanding the effects of specific phenomena such as reflector perforations and the combined modes of heat transfer [19, 20]. The group developed at Lockheed during this time continued to produce significant work on MLI, such as testing and analyzing performance at low temperatures (between 4 and 77 K) [21]. Nast published a fairly comprehensive review of their MLI-based work in 1993 [22].

Since the mid-1970s, cryogenic engineering for aerospace application saw a sharp decline in the quantity of research. Much of the work that did occur focused on the development of the specific Centaur upper stage for the Space Shuttle, which was cancelled after the Challenger accident in 1986 [23]. In the late 1980s, Mohling led a group of Ball Aerospace engineers in developing MLI systems for possible long duration Air Force satellites [24]. This project was cancelled in 1989 before a true demonstration could be completed. However, a fully comprehensive report on the development and fabrication of the test article was given to AFAL at contract termination [25]. This effort focused on the small pieces that can make or break a

true MLI system. Structural and fluid penetrations, insulation blanket seams, attachment to large tank areas, and system construction (human vs. machine, as well as ease of assembly) were a few of the main areas studied with each topic being thoroughly modeled and considered from multiple aspects. Many aspects of the MLI blankets were allowed to depart from perfect performance in order to develop a more repeatable method of construction and application.

Many groups studied the effects of layer density on MLI throughout the years preceding and following Dr. McIntosh's innovation. The subject of variable density multilayer insulation (VD-MLI) was pioneered by McIntosh in the early 1990s [2]. The theory behind variable density MLI is that because there is an optimal density for MLI as a function of both boundary temperatures, a more optimal solution exists if the MLI system is split into multiple sections or segments. Hyde [26], Stuckey [27], Fredrickson [11], and Spradley [21] have each shown analytically based graphs that suggest an optimal layer density for different systems. This work led to the variable density MLI testing on the SMiRF [28] and the MHTB [29]. While testing performed on the SMiRF does not appear to match predicted results, testing performed on the MHTB suggested that VD-MLI cut the mass of the blanket in half. In fact, the many tests run on the MHTB over the course of the approximately 15 years that it was insulated has led to many to consider VD-MLI to be a superior form of MLI and an advancement of MLI [30].

Calorimeters

When dealing with cryogenic fluids, there are two general types of calorimeters: Boil-off calorimeters, which use the known heat of vaporization of the fluid at a given saturation condition in conjunction with a measured mass or volumetric flow, and electrical calorimeters

which measure the heater power required to maintain a steady-state flow of heat energy. Both types of calorimeters have been around since the 1960s in a variety of geometries, mainly flat-plate and cylindrical.

Currently, the majority of calorimeters that use electrical power based systems are of a flat plate configuration. These include the calorimeters located at Ames Research Center (flat plate), Lockheed Martin – Palo Alto (flat plate), Sierra Lobo (flat plate), and Florida State University (cylindrical).

Steady state electrical calorimeters work controlling heaters to maintain a constant temperature on the warm boundary of the insulation; thus the heater power is measured. By maintaining both boundary temperatures at constant values, the power required by the heater to maintain the warm boundary is the power that is going through the insulation. This type of test is called a guarded hot plate and conforms to ASTM-C177. The design and operational challenge about such a system is making sure the system is completely isolated so that the heater power does solely traverse through the test insulation and not in any other direction; this lateral isolation is done by having a guard heater, similar to guard fluid tanks in boil-off calorimetry. Other systems are transient in nature and can measure both the thermal conductivity and the thermal capacitance of the insulation system by monitoring the system temperatures when a set power is applied (either cold or warm).

The system at Ames Research Center (ARC) is designed to use cryocoolers that maintain the insulation sample cold boundary at any temperature between 4 K and 290 K (no liquid is involved). This system is unique in that it places the warm boundary heater in the middle of two

flat plate test specimens in order to force all of the heat to go through the test specimens. The ARC calorimeter also allows gas to be inside of the insulation sample during testing if desired. A schematic of the ARC calorimeter is shown in Figure 1 [31]. The Lockheed Martin system used heaters on both side of the insulation that were attached to plates that whose temperatures were could be conditioned by cryogenes on both sides, thus by varying the fluid and tank pressure a much wider test conditions, a schematic of the double electrical calorimeter is shown in Figure 2 [17]. Sierra Lobo [32] uses liquid hydrogen to maintain the cold boundary on their system, which is very similar to the aforementioned system at Lockheed Martin and one that was used at Glenn Research Center during the 1970s [33]. The calorimeter in use at Florida State University (FSU) is similar to the system at Ames Research Center in that it uses a cryocooler to maintain the cold boundary; however, the cold temperature limit is approximately 10 K as opposed to 4 K at ARC. The calorimeter at FSU is cylindrical in nature, but the top and bottom are not guarded and thus need to be properly insulated using the same insulation as the cylindrical length. This approach is acceptable for bulk-fill materials, but presents challenges for testing MLI [34]. Boroski developed a similar calorimeter at Fermi National Accelerator Laboratory for testing MLI as low as 20 K [35]. This calorimeter was mainly used for determining heat fluxes through insulation designed for low temperature superconducting cables.

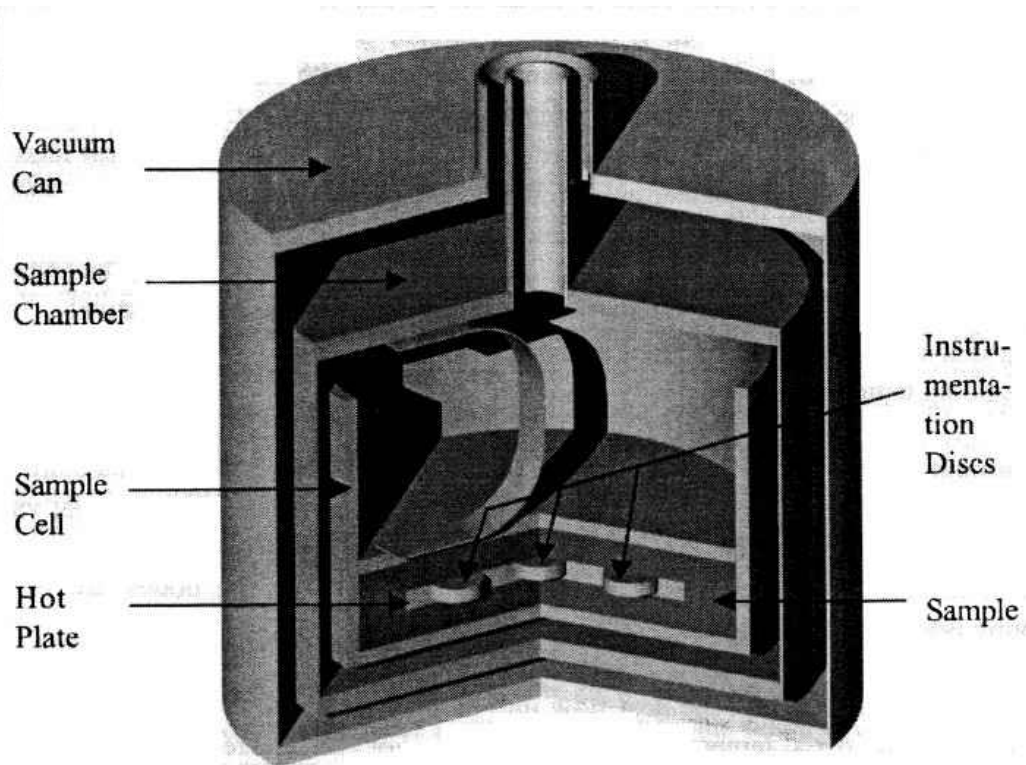


Figure 1: Ames Research Center Calorimeter (Courtesy of NASA) [31]

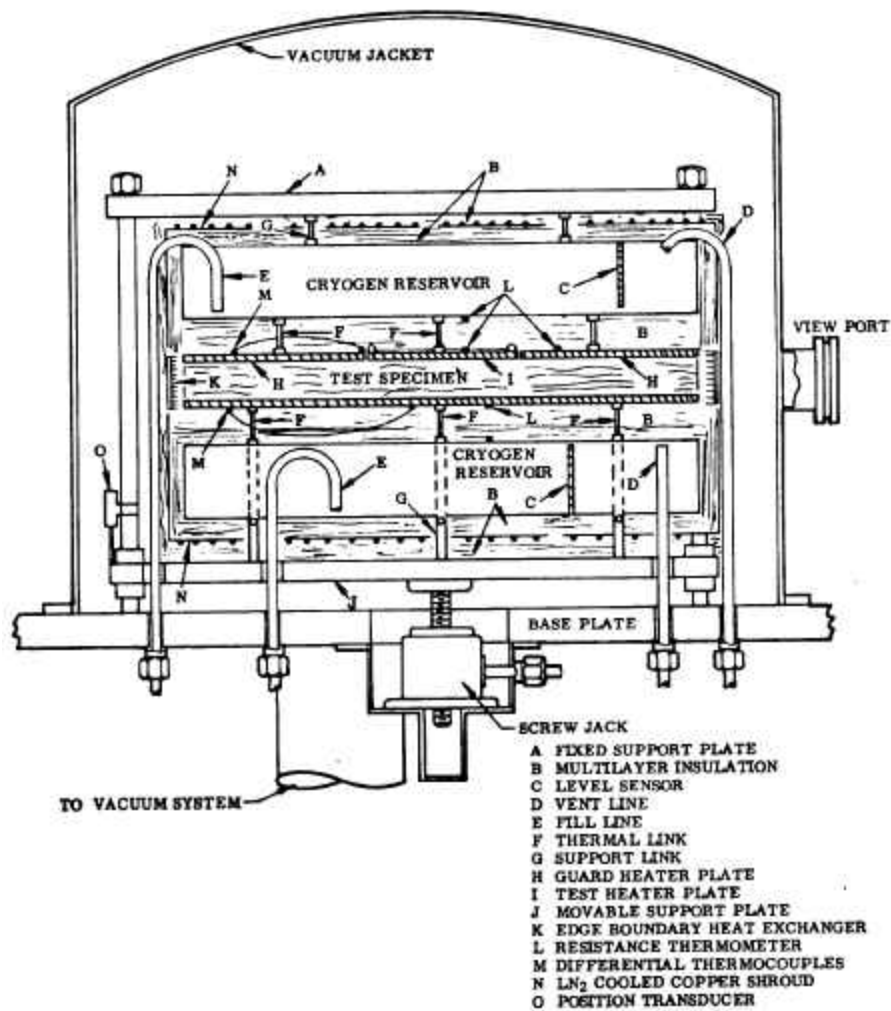


Figure 2: Lockheed guarded flat-plate electrical calorimeter (Courtesy NASA and Lockheed) [17]

Boil-off calorimeters are also used currently in both flat plate and cylindrical form. These currently exist at Kennedy Space Center (flat plate and cylindrical), Glenn Research Center (cylindrical), Europe (cylindrical), University of New Hampshire (cylindrical), Japan (cylindrical), and the Indian Institute of Technology (cylindrical). Before they developed the

double electrical calorimeter, Lockheed used a flat plate boil-off calorimeter. However, with the development of the electrical calorimeter, the boil-off one was no longer needed [16].

Boil-off calorimetry uses a known fluid property (the specific energy to change phases) and a measureable quantity (boil-off mass flow rate) to measure the heat input into a particular system. The known fluid property, the heat of vaporization (h_{fg}) is known for nitrogen as a function of liquid saturation temperature and pressure. Multiplying the heat of vaporization (J/g) by the measured mass flow rate (g/s) gives the measured heat leak into the system (J/s or watts (W)). Generally, kinetic, potential, and chemical energies are neglected as they are several orders of magnitude less than the thermal energy transported through the insulation. Even within thermal energies, results of a boil-off test can be skewed by changes in liquid, vapor, or tank state. Changes in liquid temperature or pressure should be avoided at any cost. Stochl presents a thorough analysis of such phenomena in Reference [36]. Sass and Fortier noted that even the simple daily cycles of atmospheric pressure can cause 25% swings in boil-off [37]. Great lengths are taken to insure that the heat input to the system is in a certain direction in order to attempt to create one dimensional heat transfer.

The calorimeter used at the University of New Hampshire is a double guarded cylinder with small vacuum spaces in between each chamber. There are two different outer vessels depending on the material being tested, a 4.5 inch ID (3.125 inch OD of calorimeter chambers) one for containing bulk fill insulations, and then an 11.25 inch ID chamber for testing laminar or layered insulations [38]. The calorimeters at the Indian Institute of Technology (IIT) [39], Shanghai Jiao Tong University [40], and Glenn Research Center (GRC) [36] are similar in that

the two guard vessels are separated from the main test chamber with a vacuum space (literally an open gap in between the chambers). However, the one at IIT has the two guard chambers connected by a fluid well (maintaining the bottom chamber at a slightly higher pressure due to the liquid head), whereas the GRC calorimeter guard chambers are connected via a highly conductive metal thermal rod in the middle. The two calorimeters also vary widely in size, the IIT calorimeter is 108 mm in diameter while the GRC calorimeter is 762 mm in diameter. Additionally, the GRC calorimeter has inverted domes on both the top and bottom of the test chamber, which add a small amount of uncertainty due to the fluid dynamics (see Figure 3). These two areas represent approximately 10% of the total test tank volume.

Ishikawajima-Harima Heavy Industries in Japan developed a double guarded cylindrical boil-off calorimeter using liquid helium on the cold side and liquid nitrogen as the warm boundary, the same calorimeter can be used with liquid nitrogen on the cold side and ambient temperatures on the outside. When using helium a correction factor of 1.157 is used to account for the energy absorbed by the gas between vaporization and entrance to the vent [41].

Cryostat-100 is the most advanced calorimeter developed by the Cryogenics Test Laboratory at the Kennedy Space Center. It was designed based on previous calorimeters [42] at Kennedy Space Center to allow for highly repeatable tests over a wide range of insulation performance. The versatility of Cryostat-100 allows not only for precise measurement of MLI systems performance at the high vacuum design point, but also at off-nominal design points, even up to ambient pressure, where gas conduction becomes the dominant mode of heat transfer

[43]. This versatility enables the testing that needs to be done to validate or repudiate the heat transfer models associated with multilayer insulation.

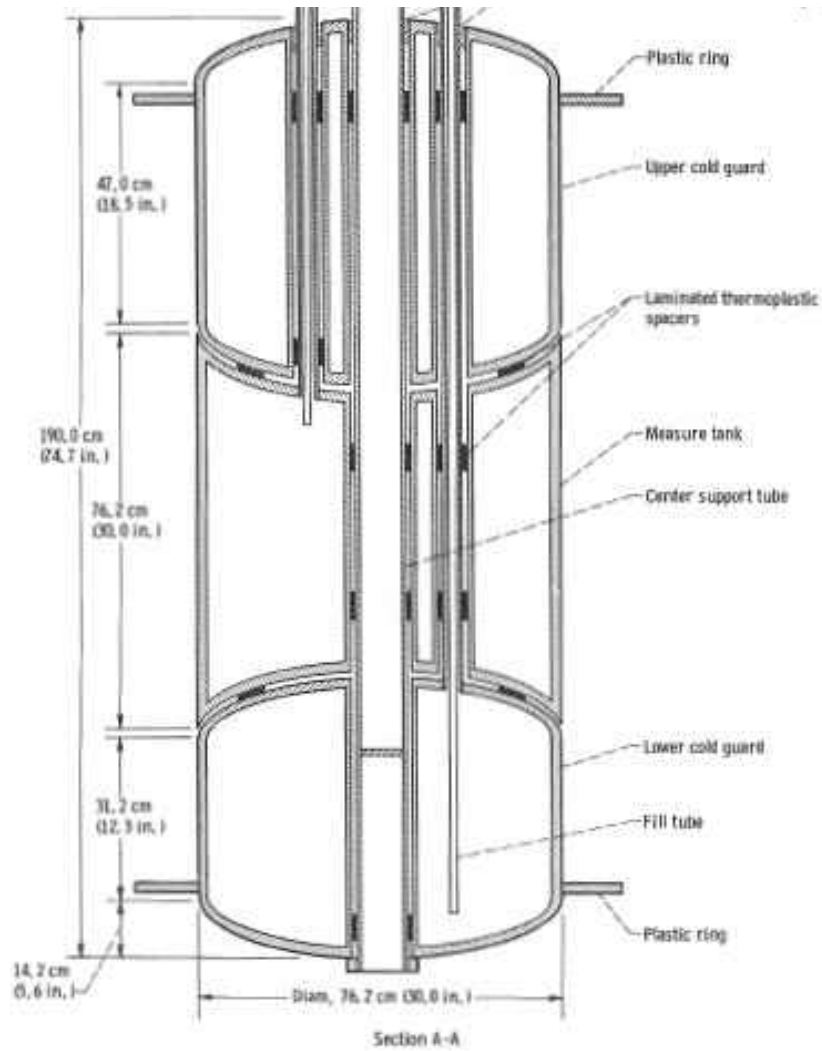


Figure 3: GRC calorimeter (Figure 3 from reference [36]), Courtesy NASA Glenn Research Center

CHAPTER THREE: THEORY

Portions of this chapter were previously published by the American Institute of Physics¹

MLI Heat Transfer

Heat transfer through multilayer insulation systems is assumed to be dominated by radiation. For this assumption to be valid, the insulation system is usually operated in a high vacuum environment with low conductance spacer material between the radiation shields. The ideal MLI system is made of floating shields that do not touch each other, however due to gravitational forces and other practical considerations this system is not feasible. A low conductivity “spacer” material is therefore placed between the radiation shields so that they do not touch and a working MLI system is produced. The solid conduction through these spacers must be accounted for in addition to the radiation between the shields. Finally, even at high vacuum levels, some gas molecules do exist between the layers of radiation shields and spacers necessitating a term for gaseous convection. All three modes of heat transfer are accounted for: the solid conduction term first followed by the radiation and gaseous conduction terms, respectively. A more thorough discussion of these modes is presented by Brogan [16] and McIntosh [2]. The general form of the empirical formulas generated in references [16] and [17] is given by equation (6) while the general form for the physics-based equations developed by McIntosh is given by equation (7).

$$q'' = \frac{C_s * \bar{N}^{2.63} (T_h - T_c) * (T_h + T_c)}{2 * (N + 1)} + \frac{C_R * \epsilon * (T_h^{4.67} - T_c^{4.67})}{N} + \frac{C_G * P * (T_h^{0.52} - T_c^{0.52})}{N} \quad (6)$$

¹ W. L. Johnson, Analytical Optimization of Multilayer Insulation Systems, in: Advances in Cryogenic Engineering, Vol 55A, American Institute of Physics, Melville, NY, 2010, pp. 804-811.

$$q'' = \frac{\sigma(T_h^4 - T_c^4)}{\left(\frac{1}{\varepsilon_h} + \frac{1}{\varepsilon_c} - 1\right)} + C_1 P \alpha (T_h - T_c) + C_2 f k \frac{(T_h - T_c)}{\Delta x} \quad (7)$$

In order to minimize the dominant mode of heat transfer, radiation, more radiation shields should be used. However, within a fixed thickness, more radiation shields mean less distance between the shields, and therefore more conduction between the shields through the spacers. As noted by Barron [44], Hyde [26], and Stuckey [27], for every MLI system there is a layer density where heat transfer is minimized. This layer density will be the same for all thicknesses given that the boundary conditions and material stay the same. The balance point in a real MLI system is between the solid conduction through spacers and the number of radiation shields for a given thickness. This analysis can be carried to its obvious conclusion that for every layer within an MLI system there is an optimal layer density. This approach is the basic premise of VD-MLI.

A few points of clarification are needed before proceeding further. First, it is well understood that decreasing the layer density while maintaining a constant number of radiation shields/layers will asymptotically decrease the heat flux through a flat plate, when the test chamber is at high vacuum. This result is due to the effects of decreasing thermal contact of the radiation shields and increasing conduction length of the spacers (an effect predicted by Fourier's law) between layers. Figure 4 shows heat flux for MLI with a constant number of layers for several published curve fit equations for varying layer densities at fixed boundary conditions of 293 K and 20 K. It is also important to note that, in theory, simple radiation models do not account for the layer density. The model includes floating shields that never touch and are separated by vacuum only.

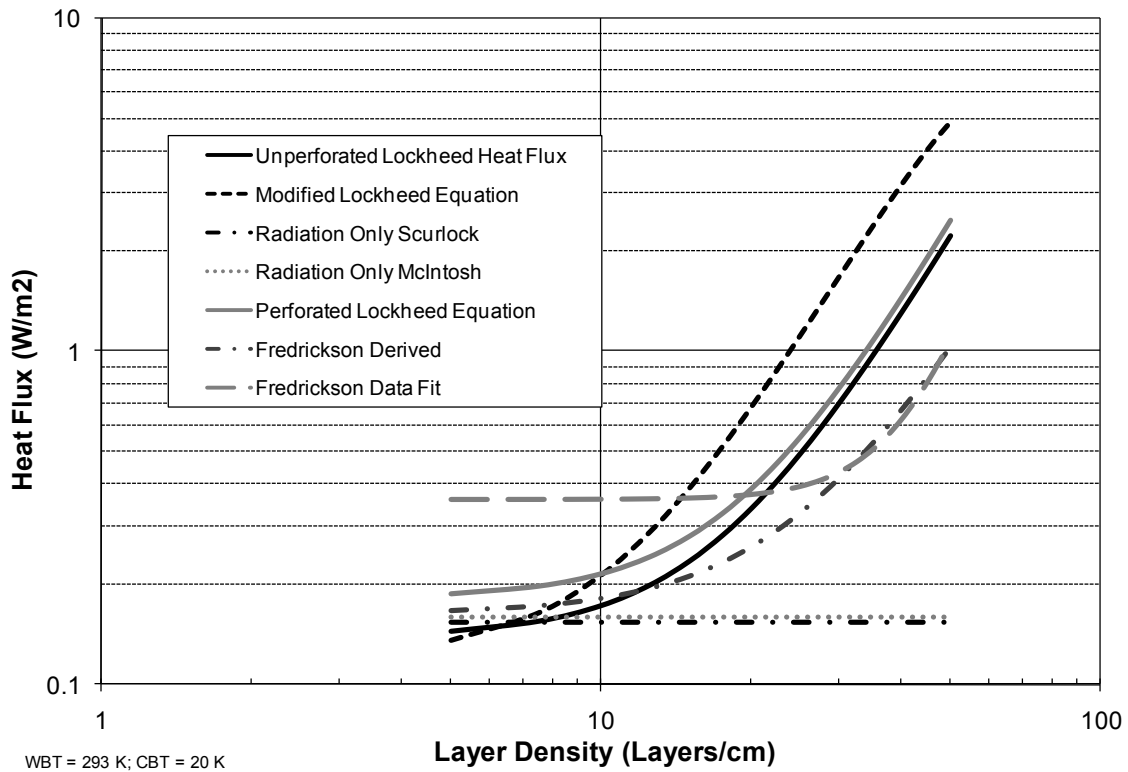


Figure 4: Heat flux as a function of layer density with a constant number of layers [1, 2, 11, 16, 17, 45]

As shown in Figure 4, it appears that the lower the density of the MLI, the lower the heat leak. However, this effect is offset by the increasing thickness of the blanket as the space between the layers increases. Seeing how every MLI blanket has a finite thickness, the thickness must be treated as finite, thus decreasing the layer density must either increase the thickness or else decrease the number of layers. Figure 5 shows the heat flux for MLI with a constant thickness for the same empirical equations. Figure 5 shows that for the same conditions as in Figure 4, with the exception of holding a constant thickness instead of the number of layers, there is a minimum point for each of the published data curve fits. That minimum point is generally where conduction begins to take over as the dominant heat transfer mode and the curve

breaks from the theoretical radiation lines. Again, it should be noticed that the theoretical radiation heat transfer only (the floating shield concept) is independent of layer density (at a constant thickness, increasing the layer density increases the number of shields, so the constant downward slope is due to the increased number of shields).

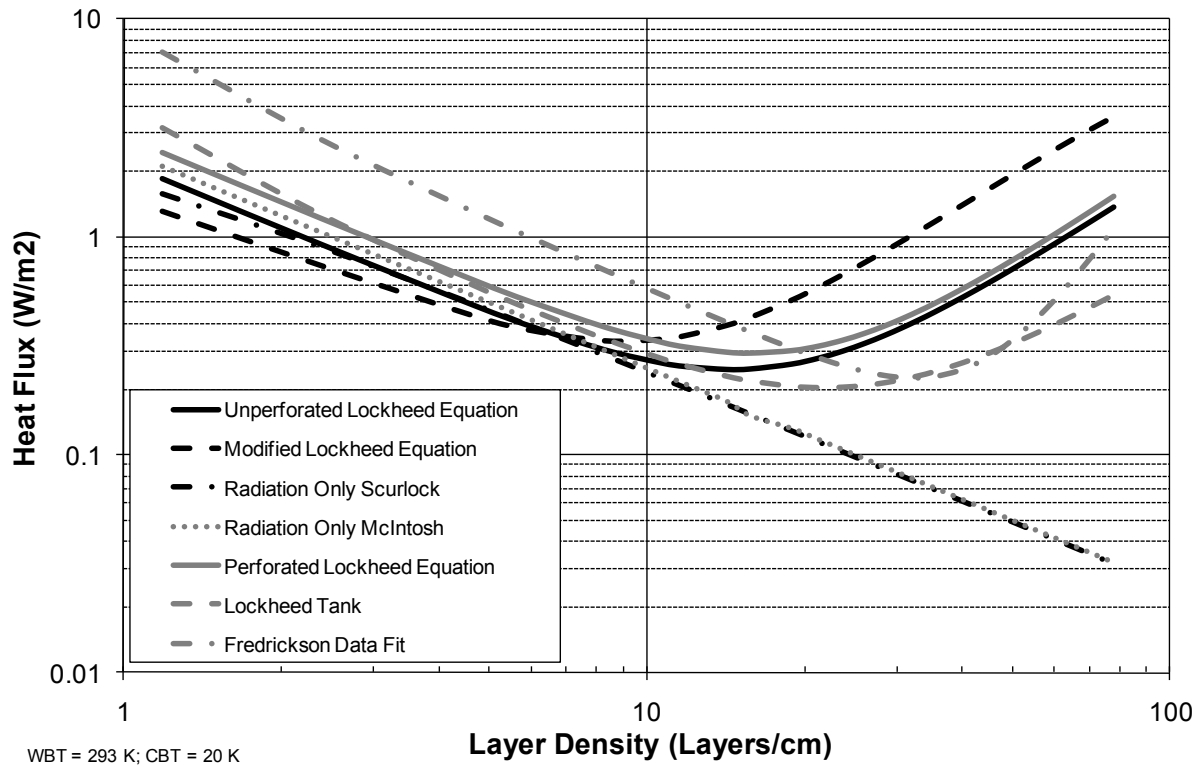


Figure 5: Heat Flux as a function of layer density for a constant thickness (25.4 mm) [1, 2, 11, 16, 17, 45]

In all the figures below, “Unperforated Lockheed” refers to unperforated double aluminized mylar radiation shields with silk net spacers, Reference [17], equation (4-14). “Perforate Lockheed” refers to the S604 perforation pattern on double aluminized mylar with silk net spacers, Reference [17], equation (4-18). The “Modified Lockheed Equation” refers to Reference [45], equation (13).

Figure 6 shows the heat flux, thermal conductivity, and estimated mass as a function of layer density for a constant number of layers. As previously shown in Figure 4 and Figure 5, the heat flux decreases exponentially with the number of layers in the MLI system. However, when the heat flux is normalized to thickness (thermal conductivity) there is a minimum. Interesting in comparison is the mass of the insulation system, which decreases asymptotically as the layer density increases. The mass decreases exponentially as the layer density increases; this trend occurs because the surface area for each individual layer is decreased when the differential between the layers is decreased in a non-flat plate application (i.e. a real tank). In the later derivations, the mass of the blanket is not taken into account, though it could be included through a complex set of equations to relate MLI blanket areal density to layer density with a known tank surface area. NASA has recently developed a FORTRAN program that is capable of performing such analysis [46].

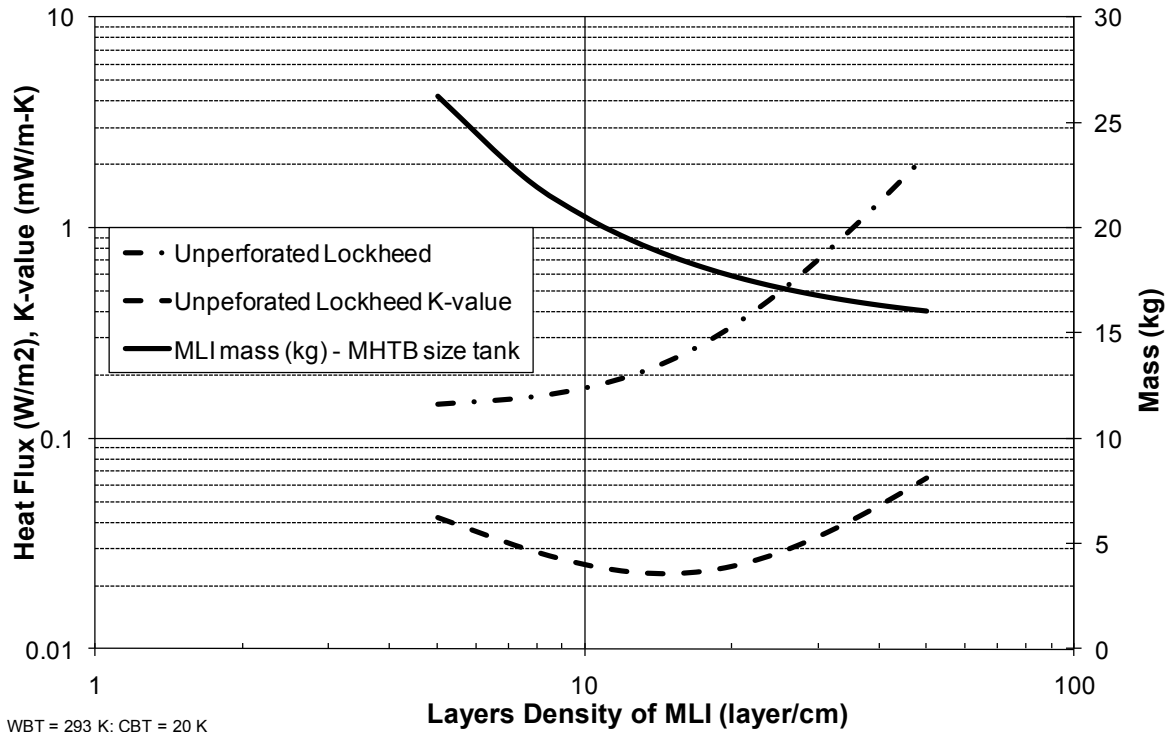


Figure 6: Heat Flux, Thermal Conductivity, and Estimated Mass for MLI as a function of Layer Density with 40 shields [1, 17]

Layer Density Optimization

Quasi-empirical equations such as those from references [17] and [45], contain both layer density (\bar{N}) and the number of layers (N) in them. In order to make the equations a function of layer density only, the equations for heat flux (q , Q/A) are converted to an effective thermal conductivity, k . As shown in Figure 7, the first derivative can then be taken with respect to layer density and set equal to zero. Solving for layer density yields an equation for the minimum heat flux normalized to thickness. For example, the process will be demonstrated on the Perforated Lockheed equation for double aluminized mylar and Dacron net, where the mylar is 0.55% open

due to perforations (reference [17] eq. 4-18). First, the heat flux is given by the following equation:

$$q'' = \frac{C_s * \bar{N}^{2.63} (T_h - T_c) * (T_h + T_c)}{2 * (N + 1)} + \frac{C_R * \varepsilon * (T_h^{4.67} - T_c^{4.67})}{N} + \frac{C_G * P * (T_h^{0.52} - T_c^{0.52})}{N} \quad (8)$$

where C_s , C_G , and C_R are the coefficients of solid conduction, gas conduction, and radiation heat transfer, ε is the emissivity of the radiation shields, T_h and T_c are the cold and warm boundary temperatures respectively, and P is the environmental pressure (for $P \leq 10^{-4}$ Torr, or in the free molecular flow regime).

Using Fourier's law (equation (9)), and assuming that the number of layers is sufficiently large (equation (10)), the equation for heat flux can be transformed into an effective thermal conductivity as given in equation (11).

$$k = q'' * \frac{\Delta x}{\Delta T} \quad (9)$$

$$N \approx N + 1 \quad (10)$$

$$k = \frac{C_s * \bar{N}^{2.63} (T_h - T_c) * (T_h + T_c) * \Delta x}{2 * N * (T_h - T_c)} + \frac{C_R * \varepsilon * (T_h^{4.67} - T_c^{4.67}) * \Delta x}{N * (T_h - T_c)} + \frac{C_G * P * (T_h^{0.52} - T_c^{0.52}) * \Delta x}{N * (T_h - T_c)} \quad (11)$$

This equation for thermal conductivity can then be simplified using equation (12) and algebra to obtain equation (13).

$$\bar{N} = \frac{N}{\Delta x} \quad (12)$$

$$k = C_s * \bar{N}^{1.63} * \frac{T_h + T_c}{2} + \frac{C_R * \varepsilon * (T_h^{4.67} - T_c^{4.67})}{(T_h - T_c) * \bar{N}} + \frac{C_G * P * (T_h^{0.52} - T_c^{0.52})}{\bar{N} * (T_h - T_c)} \quad (13)$$

Taking the first derivative of equation (13) yields:

$$\frac{\partial k}{\partial \bar{N}} = 0.815 C_s * \bar{N}^{0.63} * (T_h + T_c) - \frac{C_R * \varepsilon * (T_h^{4.67} - T_c^{4.67})}{(T_h - T_c) * \bar{N}^2} - \frac{C_G * P * (T_h^{0.52} - T_c^{0.52})}{\bar{N}^2 * (T_h - T_c)} \quad (14)$$

In order to solve for a critical point for the equation, the first derivative is set to zero, then solved for the critical point, the optimal layer density.

$$\frac{\partial k}{\partial \bar{N}_{opt}} = 0 \quad (15)$$

$$\bar{N}_{opt} = \left[\frac{C_R * \varepsilon * (T_h^{4.67} - T_c^{4.67}) + C_G * P * (T_h^{0.52} - T_c^{0.52})}{0.815 C_s * (T_h^2 - T_c^2)} \right]^{\frac{1}{2.63}} \quad (16)$$

Equation (17) shows that when all coefficients, Cr, Cs, and Cg are positive, the second derivative will always be positive. This result means that the critical point solved for in equation (16) is indeed a minimum according to the second derivative rule.

$$\frac{\partial^2 k}{\partial \bar{N}^2} = \frac{0.513 C_s * (T_h + T_c)}{\bar{N}^{0.37}} + \frac{2 * [C_R * \varepsilon * (T_h^{4.67} - T_c^{4.67}) + C_G * P * (T_h^{0.52} - T_c^{0.52})]}{(T_h - T_c) * \bar{N}^3} \quad (17)$$

The equations derived in this manner are functions only of the materials (C_s , C_G , C_R , ε) and environment (T_h , T_c , P).

$$q''_{\min} = \frac{C_s * \bar{N}_{opt}^{2.63} (T_h - T_c)(T_h + T_c)}{2 * (N + 1)} + \frac{C_R * \varepsilon * (T_h^{4.67} - T_c^{4.67})}{N} + \frac{C_G * P * (T_h^{0.52} - T_c^{0.52})}{N} \quad (18)$$

Because the layer density is an input for these equations, the optimized density can be inserted back into the equations to solve for the heat flux as shown in equation (18). Similar equations (19) can be derived for other equations, such as the Modified Lockheed Equation, developed at MSFC, with different coefficients [45]. The results of these two equations are shown in Figure 7 plotted over a wide range of warm boundary temperatures and various cold boundary temperatures that are associated with commonly used cryogenes.

$$\bar{N}_{opt,MLE} = \left[\frac{C_R * \varepsilon * (T_h^{4.67} - T_c^{4.67}) + C_G * P * (T_h^{0.52} - T_c^{0.52})}{1.63 C_s * (T_h - T_c)} \right]^{\frac{1}{2.63}} \quad (19)$$

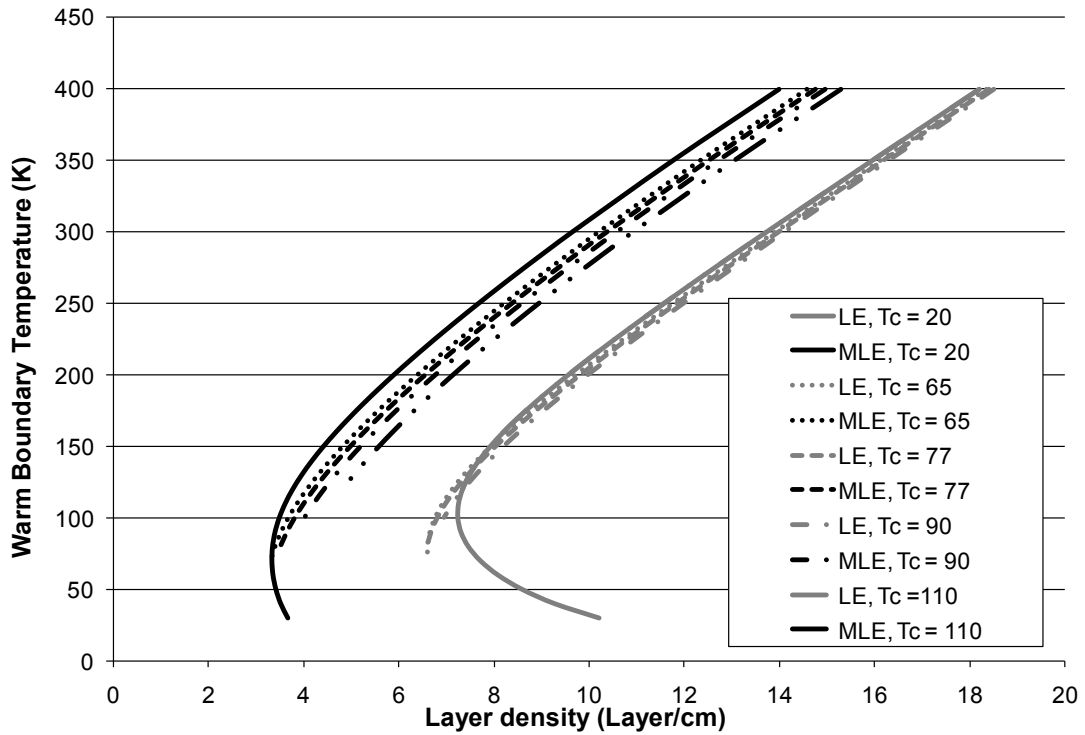


Figure 7: Optimal Layer Densities for Perforated Double Aluminized Mylar and Dacron Net MLI configurations as a function of boundary temperatures for $P = 10^{-5}$ Torr [17, 45]

CHAPTER FOUR: TEST METHODOLOGY

Various experimental test methodologies have been used to determine the heat transfer through MLI; the one used for this study is boil-off calorimetry.

Experimental Setup

Testing was performed using Cryostat-100 according to standard laboratory test procedures [47]. Cryostat-100, located at the Kennedy Space Center, is a cylindrical boil-off calorimeter including three liquid nitrogen tanks. The main liquid nitrogen tank measures the heat flux through the insulation and is guarded by liquid nitrogen tanks kept at the same pressure as the main measure tank. This back pressure can either be allowed to vary with the local atmospheric pressure, or it can be controlled by a back pressure chamber which acts to damp out the variations due to local tides and weather patterns.

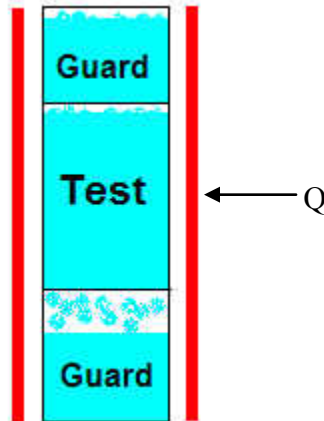


Figure 8: Absolute Cylindrical Boil-off Calorimetry

The main measurement of a boil-off calorimeter is the mass flow rate of the boiling vapor. The expansion ratio of nitrogen from saturated liquid to saturated vapor is over 100 (one

cubic meter of liquid produces 100 cubic meters of saturated vapor). As the liquid boils (or in most cases of very low heat flux it evaporates; that is, no bubbles are formed) it forces itself out of the vent line due to small increases in pressure. Thus a small amount of the vapor replaces the volume of the liquid that is vaporized and the rest leaves the chamber via the vent line and it measured. Equation (20) shows the governing equation for boil-off calorimetry. However, because the expansion ratio from liquid to vapor is so large, the liquid density is roughly equal to the differential density between liquid and gas. Thus the error in assuming that portion of the equation is less than 1% (for nitrogen it is a 0.6% error) allows simplification of equation (20) to equation (21).

$$\dot{Q} = \dot{m}h_{fg} \left(\frac{\rho_f - \rho_g}{\rho_f} \right) \quad (20)$$

$$\dot{Q} = \dot{m}h_{fg} \quad (21)$$

Additional terms are often needed to account for miscellaneous heat transfer effects. Such heat transfer occurs when guard chambers are not exactly isothermal, or if there is two-dimensional heat transfer through the test article. If a temperature controlled cold wall is available and safe to use, this miscellaneous heat transfer can be determined by running a null test as demonstrated by Sumner [33]. In some conditions, especially when the liquid level is low, the temperature of the gas at the test chamber exit should be measured with the appropriate correction factor shown in equation (22). This measurement accounts for any superheating that may occur after the fluid changes phases, but before it leaves the test chamber [48].

$$\dot{Q} = \dot{m}(h_{fg} + h_{T_{exit}} - h_g) = \dot{m}(h_{T_{exit}} - h_f) \quad (22)$$

Original attempts at boil-off testing used extruded copper foams and copper wool within high conductivity aluminum tanks to try to maintain isothermal conditions throughout the test and guard chambers. [36] This breaks up the normal stratification that is caused by additional hydrostatic pressure within the liquid as a function of liquid height, but complete stratification is difficult to achieve in standard practice. More recently, several stainless steel calorimeters have been developed that allow for stratification to occur but provide thermal stability over long time periods. However, analysis should be done to determine if the thermal effects of this stratification require another correction factor associated with the thermal capacitance of the liquid. For Cryostat-100, the correction factor is less than 0.5% as shown in Figure 9. A complete uncertainty analysis was performed on Cryostat-100 previously, and the total uncertainty was found to be less than 5% [49].

Top of the Test Chamber	Bottom of the Test Chamber	
$P_1 := 102 \cdot 10^3 \text{ Pa}$	$L := 0.5588 \cdot \text{m}$	$\rho := 810.8 \frac{\text{gm}}{\text{liter}}$
$T_1 := 77.42 \text{ K}$	$g = 9.807 \frac{\text{m}}{\text{sec}^2}$	$P_2 := P_1 + \rho \cdot g \cdot L$
$h_1 := -121.9 \frac{\text{joule}}{\text{gm}}$		$P_2 = 1.064 \times 10^5 \text{ Pa}$
		$T_2 := 77.8 \cdot \text{K}$
$h_2 := 77.2 \frac{\text{joule}}{\text{gm}}$		$h_3 := -121.2 \cdot \frac{\text{joule}}{\text{gm}}$
Enthalpies generated from RefProp V8		
$h_{fg} := h_2 - h_1$		$h_{sc} := h_3 - h_1$
$h_{fg} = 1.991 \times 10^5 \text{ Sv}$	note: $\text{Sv} = \text{J/kg}$	$h_{sc} = 700 \text{ Sv}$
$err := \frac{h_{sc}}{h_{fg}}$		
Total error associated with stratified liquid		
$err = 3.516 \times 10^{-3}$		

Figure 9: Error Calculation for Stratified Cryostat-100

Using Fourier's equation (9), a k-value, equation (23), can be defined within the cylindrical coordinates of the calorimeter as shown in equation (24).

$$k = q \frac{\Delta x}{\Delta T} \quad (23)$$

$$k = \frac{m h_{fg} \ln(r_o/r_i)}{2\pi L \Delta T} \quad (24)$$

To determine heat flux, the logarithmic mean area must be determined. For a cylinder, this value is determined by equation (25) and the heat flux is then determined by the power input divided by the logarithmic mean area.

$$A_{lm} = \frac{A_{outer} - A_{inner}}{\ln(A_{outer}/A_{inner})} = 2\pi L \frac{r_o - r_i}{\ln(r_o/r_i)} \quad (25)$$

For further insight into the performance and testing of the samples, thermocouples are placed throughout the thickness of the MLI. This approach allows for the determination of the temperature profile of the blanket as a function of thickness. Generally, more thermocouples are placed on the layers closer to the cold mass. Because radiation is a function of T^4 , the temperature profiles are generally highly curved, with most of the temperature gradient occurring in the first 25% of the insulation. Thermocouple locations for each test are shown in Table 3. Additionally, the interior thermocouples allow insight into the determination of steady state. Steady state can be determined to have been reached once the thermocouples begin to vary consistently with the cycling of the air conditioning within the laboratory, or varies less than the general error of the thermocouple over the course of a day. Using this method for steady state determination allows for a repeatable method of determining steady state within a boil-off calorimeter.

One cause for concern during calorimeter testing is non-one dimensional heat transfer. In a cylindrical calorimeter, this would be caused by non-isothermal layers. Because the thermal conduction of aluminum or aluminized mylar is much higher than the conduction through the MLI, thermal gradients along an individual shield could cause a large error in the data. In a previous test, 3 thermocouples were placed with roughly 12 inches between each thermocouple in order to look for any non-one dimensional temperature gradients within the MLI. These sensors were placed on the 12th out of 40 layers, where the measured temperatures were in the 160 to 200 K range depending on the residual gas pressure within the MLI. Using thermal

conductivity data for mylar (Polyethylene Terephthalate) from NIST [50] and the geometric properties of the 12th layer (see Table 1), parasitic conduction heat loads were calculated for all vacuum levels. The maximum heat load (assuming that layer 12 was the average conduction load) was less than 1 milliwatt and at high vacuum it was even lower at 0.4 milliwatt for the whole system (see Table 2). This analysis shows that indeed the testing performed on Cryostat-100 is a one-dimensional cylinder and that any edge effects that occur are minimized by the upper and lower guard chambers.

Table 1: Geometric properties of the 12th layer of A125

Diameter (m)	Distance between thermocouples (m)	Mylar thickness (m)	Heat Transfer Area (m ²)
0.178	0.305	6.35E-6	3.55E-6

Table 2: Measured conduction heat load for all vacuum pressures

Cold Vacuum Pressure (mTorr)	Mylar $\lambda(T)$ (W/m-K)	12 th layer top (W)	12 th layer bottom (W)	Total blanket top (W)	Total blanket bottom (W)
0.01	0.082	5.66E-06	5.99E-06	2.26E-04	2.39E-04
0.1	0.092	4.45E-06	1.61E-05	1.78E-04	6.44E-04
1	0.108	-1.23E-06	2.46E-05	-4.93E-05	9.85E-04
10	0.124	-2.70E-06	5.94E-06	-1.08E-04	2.37E-04
10	0.083	7.20E-06	7.98E-06	2.88E-04	3.19E-04
100	0.129	-9.42E-06	-1.41E-07	-3.77E-04	-5.63E-06
1000	0.125	-1.62E-05	2.20E-05	-6.47E-04	8.81E-04
10000	0.119	-2.45E-05	4.14E-05	-9.82E-04	1.66E-03
100000	0.104	-2.86E-05	-7.10E-07	-1.14E-03	-2.84E-05
760000	0.100	-1.87E-05	-3.98E-05	-7.48E-04	-1.59E-03

Table 3: Thermocouple placement for each test series

Thermocouple	A138 Coupon A 60 layers	A139 Coupon A 40 layers	A140 Coupon B 10 layer/cm	A141/A143 Coupon B 15 layer/cm	A142 Quest	A144 Coupon B 26 layer/cm
T1,T2, T3	Cold Boundary	Cold Boundary	Cold Boundary	Cold Boundary	Cold Boundary	Cold Boundary
T4	DAK – layer 0	DAK – layer 0	DAK – layer 0	DAK – layer 0	Layer 1	DAK – layer 0
T5	Layer 4	Layer 4	Layer 4	Layer 4	Layer 2	Layer 4
T9	N/A	N/A	Layer 8	Layer 8	Layer 10	Layer 8
T6	Layer 12	Layer 12	Layer 12	Layer 12	Layer 3	Layer 12
T7	Layer 20	Layer 20	Layer 20	Layer 20	Layer 4	Layer 20
T10	N/A	N/A	Layer 28	Layer 28	Layer 12	Layer 28
T8	Layer 36	Layer 36	Layer 36	Layer 36	Layer 8	Layer 36
T11,T12,T13 Warm Boundary	Layer 60	Layer 40	Layer 60	Layer 60	Layer 20	Layer 60

Experimental Measurement, Uncertainty, and Variability

Previously, an investigation was done into the uncertainties associated with Cryostat-100 [43]. This investigation used the least squares method to determine the total uncertainty based on the error of the different variables in the equations presented above. It was shown that the uncertainty on Cryostat-100 was approximately 4%.

In order to measure the performance of multilayer insulation blankets via boil-off calorimetry, several major categories of instrumentation are needed. Flow meters measure the volumetric flow of boil-off at standard temperature and pressure (thus a mass flow). Pressure transducers measure the vacuum pressure, both before and after filling with liquid nitrogen as well as the back pressure on the liquid nitrogen chambers. Thermocouples (silicon diodes or

resistance temperature detectors - RTDs - can also be used) measure the temperature on the cold boundary, warm boundary and other locations in between as desired.

To measure the boil-off flow, MKS type M10MB mass flow meters are used. These flow meters operate on a thermal bypass theory where a known portion of the flow is diverted through a small duct and a known heat is applied, the change in temperature of the gas indicates how much flow is going through the entire flow meter. Generally these flow meters have a published 1% of full scale error associated with them and are best used between the 20% and 80% full scale output. At high vacuum, the test chamber of Cryostat-100 often has a flow of less than 50 sccm, while the guard chambers are close to 200 sccm. At no vacuum, the test chamber can have flows in excess of 15,000 sccm with comparable flows on the guard chambers. This wide range of flow creates the need to have multiple ranges of flow meters available.. The flow meters use a 15 pin D connector (five of which are active), of which three pins provide 15 VDC to the flow meter and two pins carry the output signal (0-5 V) to the data acquisition system.

Vacuum pressure is critical to understanding the gas conduction characterization, especially for MLI. In order to measure the wide range of pressures between 760 torr and 10^{-6} torr (almost 10 orders of magnitude) several different transducers are needed. MKS Baratron Type 627B are used for the bulk of measurements, they can be ordered in a variety of full scale ranges and are generally accurate to 0.25% of the reading. The Type 627B are capacitance manometers made of corrosion resistant Inconel to allow for use in multiple different gasses. Because the resolution of a Baratron is roughly 0.001% FS, a 100 Torr Baratron is generally used in concert with a 0.1 Torr Baratron, this gives excellent accuracy to 10^{-4} Torr. At pressures

below that, a Granville Phillips ion gauge is used. A full range gage by Pfeiffer is also used to provide backup confirmation of the primary gages and to facilitate operations of the vacuum system.

To measure the warm and cold boundary temperatures, Type E thermocouples are used. Type E thermocouples provide the greatest voltage differences between temperatures of any type of thermocouple in the cryogenic temperature range. Typical errors on thermocouples are 2 K or less, which is less than 1% of the total temperature difference across the multilayer insulation (typically 215 K). In addition to warm and cold boundary temperatures, thermocouples are used to measure various layers in between the two, typical thermocouple placements for different numbers of layers are shown in Table 3.

Previous testing with Cryostat-100 had exhibited a twelve hour cyclical trend in the boil-off flow rates. This periodic variation is now known to be caused by fluctuations in the local air pressure due to the atmospheric tides as has been previously suggested by Sass and Fortier for other boil-off measurement systems [37]. In order to mitigate or dampen this effect, a back pressure control system was recently set up for Cryostat-100 (see Figure 10). The back pressure control system has a gaseous nitrogen feed with a control valve attached to a pressure transducer (MKS Baratron Type 627D capacitance manometer). A control box including proportional, integral, and derivative (PID) control provides the necessary link between the pressure transducer and the control valve. This system effectively dampened the effect and allowed test times to be reduced. The small atmospheric changes having a large effect on the condition of the

boil-off cryogen illustrate the sensitivity and difficulty in measuring extremely small rates of heat energy, such as below 1 W/m^2 .



Figure 10: Cryostat-100 backpressure control system for dampening the effect of the atmospheric tides on the boil-off cryogen.

The back pressure control system was used to damp out the 12 hour tidal cycles. Figure 11 shows a comparison of the boil-off flow rates for A138 and A139. On the left side, A138 did not have the back pressure control system in place; however the right side, A139, did have the back pressure control system in place. The y-axis on both graphs is identical; this chart shows that the amplitude of the variation was reduced from 5 sccm to less than 1 sccm. All subsequent tests were run with the back pressure control system in place, making the data analysis easier and reducing the time required for a given test. With the back pressure control system in place, the variability of the flow within the tests is generally within 10% as the holding chamber is not

sufficiently large to prevent slight changes in back pressure that correlate with changes in the weather as well as the normal operation of the air conditioning system in the laboratory.

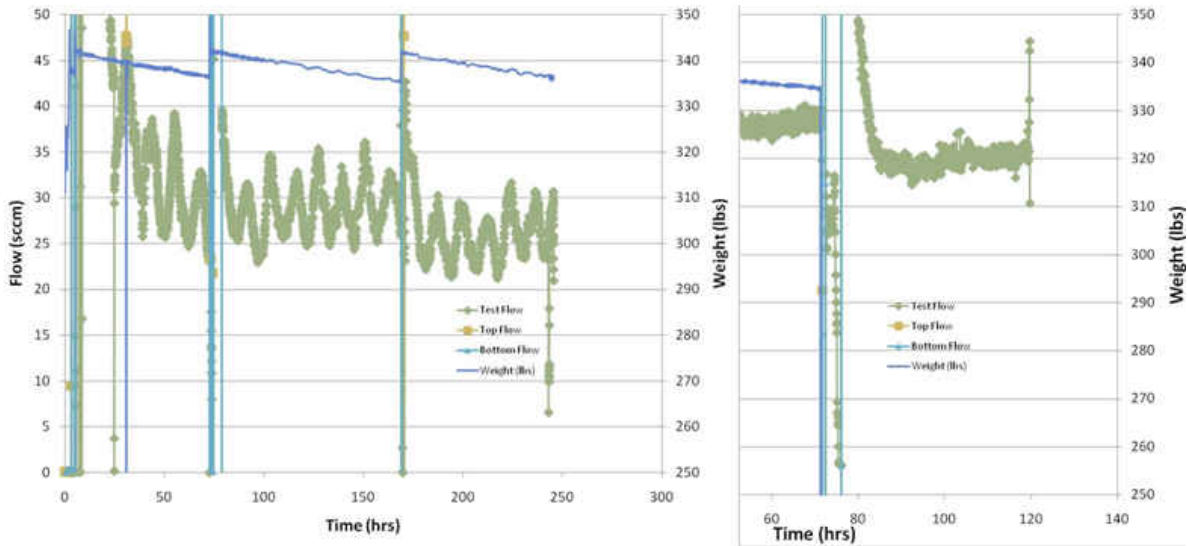


Figure 11: Comparison of Flow Variation before and After Installation of Back Pressure Control System

Insulation Specimens

Two MLI “coupon” test articles were procured from Ball Aerospace for testing on Cryostat-100. The first coupon is representative of the insulation installed on the MLSTC test tank at GRC by Ball Aerospace personnel and serves to give an approximate heat leak through the MLSTC insulation. The second coupon is a calorimetric test sample intended to test the heat transfer effects of changing the layer density of an MLI blanket. A third coupon was provided by Quest Product Development Corporation as a deliverable from their Phase II SBIR, *Integrated MLI: Advanced Thermal Insulation Using Micro-Molding Technology*, contract NNC08CA13C [51].

The Ball first coupon, Coupon A, consists of 60 layers of alternating double aluminized Mylar (DAM) and Dacron netting. Every four layers are joined to form a “sub-blanket” where the outer aluminized Mylar is 1 mil thick (0.001”) and the other three reflectors are 0.25 mil thick (0.00025”). Each reflector is separated by Dacron B4A netting. There are a total of 15 “sub-blankets.” A 0.25 mil layer of double aluminized mylar was placed under the MLI to better represent a shiny tank surface (Cryostat-100’s cold mass outer surface is painted black to prevent optical interference in most calorimetric situations). The sub-blankets were held together by pieces of Velcro sewn into the 1 mil piece of DAM along the seams (see Figure 12); these seams were purposely staggered around the circumference of the cold mass to prevent bulges in the insulation blanket.

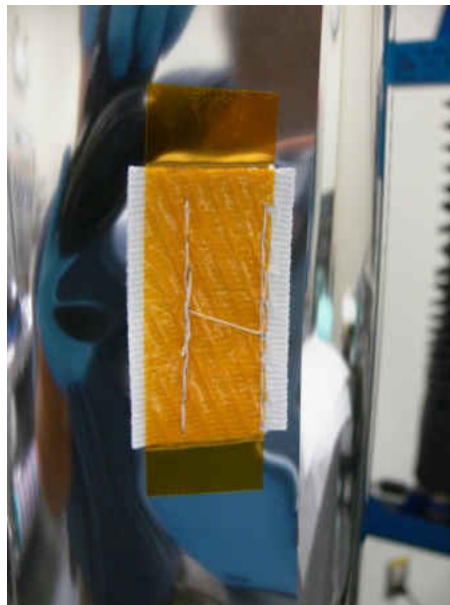


Figure 12: Typical Velcro attachment for MLI Coupon A.

The second coupon, Coupon B, is nearly identical to Coupon A with several notable exceptions. The sub-blankets are held in place by pieces of tape instead of Velcro; this

attachment method brought up the possibility of thermal bridging (heat conduction) between layers. However, bridging was minimized by using pieces of Dacron netting on the tape to minimize conduction where the tape was applied across the layers (see Figure 13). In order to keep the sub-blanket layers together, small plastic tags were inserted through each layer. These tags, commonly known as garment tags, are minimal in cross sectional area.

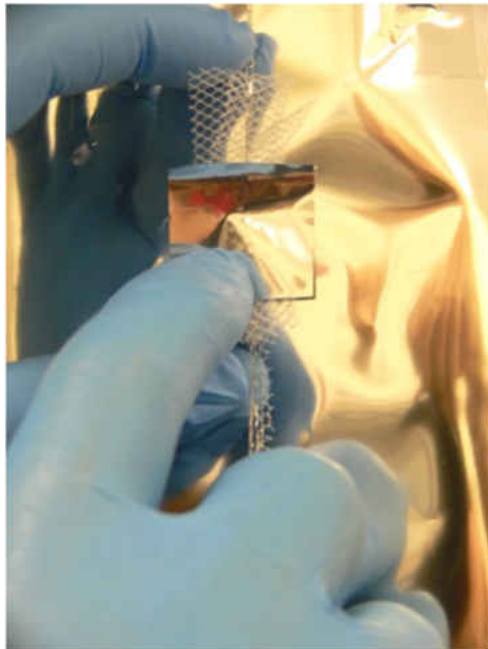


Figure 13: Typical tape attachment on MLI Coupon B using a small piece of Dacron netting to minimize thermal bridging.

Quest has developed an “integrated” multilayer insulation (IMLI) in which there is no spacer layer. Instead, the spacing of the radiation shields is maintained by proprietary micro-molded polymer stands that are spaced out over the radiation shields and glued to both of its boundary shields (see Figure 14). As a final deliverable to their Phase II SBIR project, *Integrated MLI: Advanced Thermal Insulation Using Micro-Molding Technology*, Contract

NNC08CA13C, Quest was required to produce a sample of IMLI that was fitted to Cryostat-100 dimensions.



Figure 14: IMLI plastic spacer grid

IMLI is currently designed for a layer density of 5.5 layers/cm (14.1 layer/in). Quest uses one mil thick double aluminized Mylar (DAM) for the main radiation shield layers in the insulation system to give rigidity to the layers and prevent film to film contact. The spacers between reflective layers are proprietary micro-molded polymer supports. The test sample was divided into two sub-blankets, each consisting of 10 layers (see Figure 15). The two sub-blankets were connected both by tension and by Velcro strips that ran around the circumference. Each sub-blanket was taped closed on the outer layer; however, interstitial layers were interleaved at the seam.



Figure 15: IMLI Cryostat-100 layup

CHAPTER FOUR: RESULTS AND DISCUSSION

Six different test article (coupon) configurations were tested over the course of seven test series. These test series covered a wide range of vacuum pressures, warm boundary temperatures, and geometric parameters. The parameters from the various coupons and modifications that were used are shown in Table 4. BATC Coupon B was designed for the layer density to be changed during testing. Some coupons were not tested for the full vacuum range due to time and funding restraints, as the main goal of the test program was to determine the insulation system performance at high vacuum. For example, A138 and A139 were only tested at high vacuum and ambient pressure (no vacuum), while A140 was tested only at high vacuum and slightly degraded vacuum pressures. The four variables investigated in the study were: Number of Layers, Layer Density, Cold Vacuum Pressure, and Warm Boundary Temperature.

Table 4: Key Geometrical Parameters for MLSTC Cryostat-100 Testing

Test Series	Coupon	Number of Layers	Layer Density (layer/mm)	Thickness (mm)	Mean Area (m²)	Mass Density (kg/m³)
A138	BATC A	60	0.95	63.3	0.409	45
A139	BATC A	40	0.94	42.7	0.377	45
A140	BATC B	60	0.94	63.6	0.409	37
A141	BATC B	60	1.45	41.4	0.375	57
A142	Quest IMLI	20	0.52	38.7	0.370	21
A143	BATC B	60	1.41	42.6	0.377	55
A144	BATC B	60	2.61	23.0	0.344	95

Test Results

Summaries of the Cryostat-100 test results are shown in 5 and 6. The figures in parentheses (which are the same used in the legends of the figures) indicate the number of layers, the layer density (layer/mm), and the mass density (kg/m^3). The average measured boil-off flow rate and the corresponding total power, thermal conductivity, and heat flux are shown in addition to the cold vacuum pressure and both boundary temperatures. Results are generally shown to 3-4 significant figures except on the mass flow rates, where a minimum of three are given.

Table 5: Test results for calorimeter testing (Part I)

A138 Ball MLI 60, Coupon A (60, 0.95, 45)	Test	Flow	Qtot	k	CVP	WBT	Q/A_m	CBT
15 sub-blankets		(sccm)	(W)	(mW/m-K)	(μ)	(K)	(W/m²)	(K)
60 Layers, 0.95 layer/mm	1	25.8	0.107	0.073	0.0058	305	0.262	78
2.5 inch total thickness	2	37.3	0.154	0.088	0.0073	349	0.377	78
	3	12067	49.94	34.4	760000	303	122.2	78
A139 Ball MLI 40, Coupon A (40, 0.95, 45)	Test	Flow	Qtot	k	CVP	WBT	Q/A_m	CBT
10 sub-blankets		(sccm)	(W)	(mW/m-K)	(μ)	(K)	(W/m²)	(K)
40 layers, 0.94 layer/mm	1	35.2	0.146	0.073	0.0026	305	0.388	78
1.6 inch total thickness	2	50.7	0.210	0.088	0.004	349.5	0.557	78
	3	13387	55.4	37.38	760,000	307.5	147.1	78
A140 Ball MLI 60, Coupon B (60, 0.94, 37)	Test	Flow	Qtot	k	CVP	WBT	Q/A_m	CBT
15 sub-blankets		(sccm)	(W)	(mW/m-K)	(μ)	(K)	(W/m²)	(K)
60 layers, 0.94 layer/mm	1	32.8	0.136	0.093	0.0017	305.8	0.332	78
2.5 inch total thickness	2	33.1	0.137	0.094	0.0018	305.6	0.335	78
	3	68.2	0.282	0.193	0.106	305	0.689	78
	4	79.6	0.329	0.226	0.307	305	0.804	78
A141 Ball MLI 60, Coupon B (60, 1.45, 57)	Test	Flow	Qtot	k	CVP	WBT	Q/A_m	CBT
15 sub-blankets		(sccm)	(W)	(mW/m-K)	(μ)	(K)	(W/m²)	(K)
60 layers, 1.45 layer/mm	1	42.8	0.177	0.087	0.002	304.7	0.472	78
1.6 inch total thickness	2	42.3	0.175	0.085	0.003	304.8	0.467	78
	3	90.4	0.372	0.183	0.107	304.5	0.993	78
	4	119.6	0.495	0.242	0.303	304.4	1.321	78

Test articles A138 and A139 were tested at high vacuum (with WBTs of 305 and 350 K) and no vacuum. Test articles A140, A141 and A144 were tested at high vacuum and slightly

degraded levels of high vacuum in order to establish the curved transition region between high vacuum and soft vacuum and how it is affected by layer density at a warm boundary temperature of 305 K. Test article A142 was initially tested in the same conditions as A140 and A141, but then subsequently tested for the full vacuum range at a warm boundary temperature of 293 K. Test article A141 was then reinstalled as A143 and tested for the full vacuum range at 293 K. A majority of the CVP dependent testing was performed at a WBT of 305 K; these results are shown in Figure 16 as heat flux and Figure 17 as apparent thermal conductivity. Figure 18 (heat flux) and Figure 19 (k-value) show the high vacuum performance of multiple insulation systems at different warm boundary temperatures. The no vacuum (ambient pressure, nitrogen back-fill) performance of various systems is shown in Figure 20.

Table 6: Test results for calorimeter testing (Part II)

A143 Ball MLI 60, Coupon B (60, 1.41, 55)	Test	Flow	Qtot	k	CVP	WBT	Q/A_m	CBT
2 subblankets		(sccm)	(W)	(mW/m-K)	(μ)	(K)	(W/m²)	(K)
20 layers, 0.52 layer/mm	1	33.3	0.138	0.073	0.002	292.9	0.4	78
1.5 inch total thickness	2	56.4	0.233	0.123	0.108	292.9	0.6	78
	3	70.4	0.291	0.153	0.306	292.8	0.8	78
	4	100.5	0.416	0.219	1.0	293.1	1.1	78
	5	438.0	1.8	1.0	10.0	292.6	4.8	78
	6	2733.0	11.3	6.0	100.0	292.8	30.0	78
	7	6296.0	26.1	13.7	1074.0	292.8	69.3	78
	8	7274.0	30.1	15.8	10026.0	293.3	79.9	78
	9	7139.0	29.5	15.6	100018.0	293.0	78.3	78
	10	9780.0	40.5	21.5	760000.0	291.2	107.5	78
A144 Ball MLI 60, Coupon B (60, 2.6, 95)	Test	Flow	Qtot	k	CVP	WBT	Q/A_m	CBT
15 subblankets		(sccm)	(W)	(mW/m-K)	(μ)	(K)	(W/m²)	(K)
60 layers, 2.6 layer/mm	1	30.6	0.127	0.037	0.003	305.3	0.369	78
0.9 inch total thickness	2	31.6	0.131	0.038	0.004	305	0.380	78
	3	54.5	0.225	0.060	0.056	304.1	0.653	78
	4	60.3	0.249	0.073	0.113	304.4	0.723	78
	5	72.0	0.298	0.088	0.307	304.8	0.865	78
A142 Quest IMLI (20, 0.52, 21)	Test	Flow	Qtot	k	CVP	WBT	Q/A_m	CBT
2 subblankets		(sccm)	(W)	(mW/m-K)	(μ)	(K)	(W/m²)	(K)
20 layers, 0.52 layer/mm	1	50.7	0.210	0.097	2.50E-03	304.2	0.567	78
1.5 inch total thickness	2	54.2	0.224	0.104	7.80E-03	303.6	0.605	78
	3	114	0.472	0.219	1.00E-01	304.3	1.274	78
	4	141.4	0.585	0.271	3.00E-01	304.5	1.579	78
	5	36.7	0.152	0.074	1.20E-03	291.8	0.410	78
	6	107.1	0.443	0.216	1.00E-01	292.7	1.196	78
	7	215.4	0.891	0.436	1.00E+00	292.4	2.406	78
	8	1144	4.74	2.30	1.00E+01	294.4	12.787	78
	9	5032.4	20.8	9.98	1.00E+02	296.3	56.227	78
	10	7107.0	29.4	14.06	1.01E+03	296.7	79.406	78
	11	9278	38.4	18.36	1.00E+04	296.7	103.679	78
	12	17362	71.8	34.83	7.60E+05	293.8	193.979	78

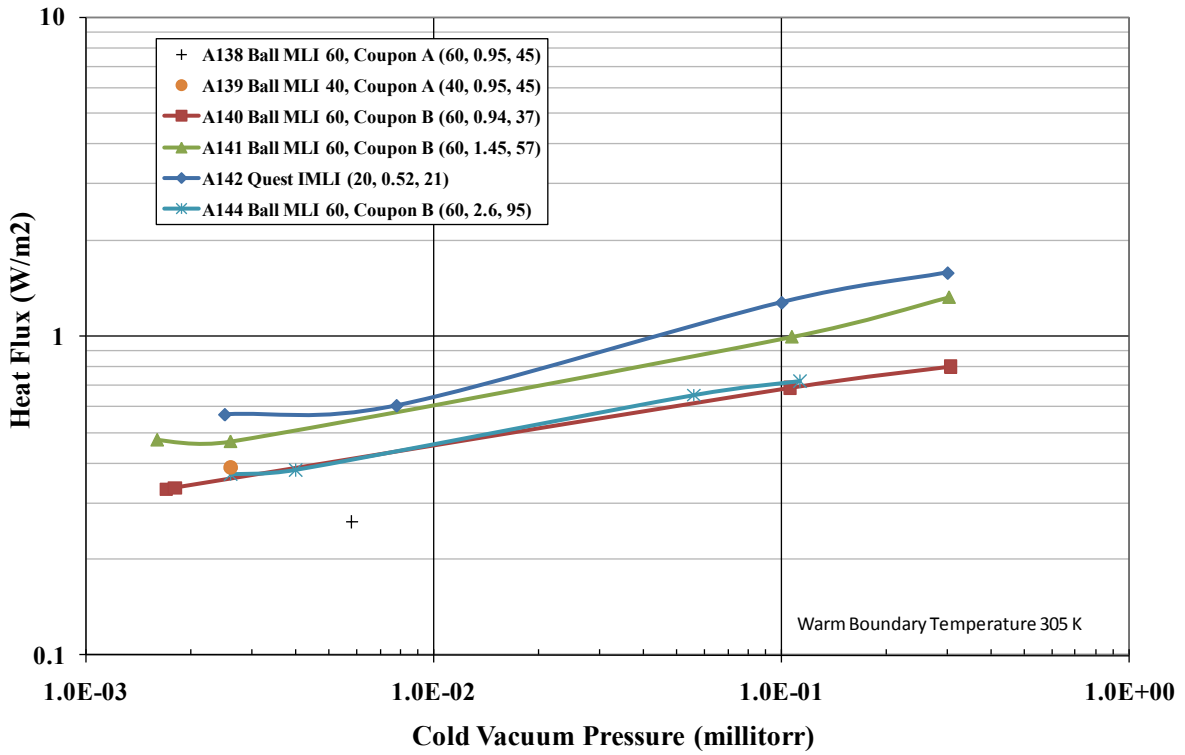


Figure 16: Heat flux as a function of CVP for various MLI systems as a WBT of 305 K

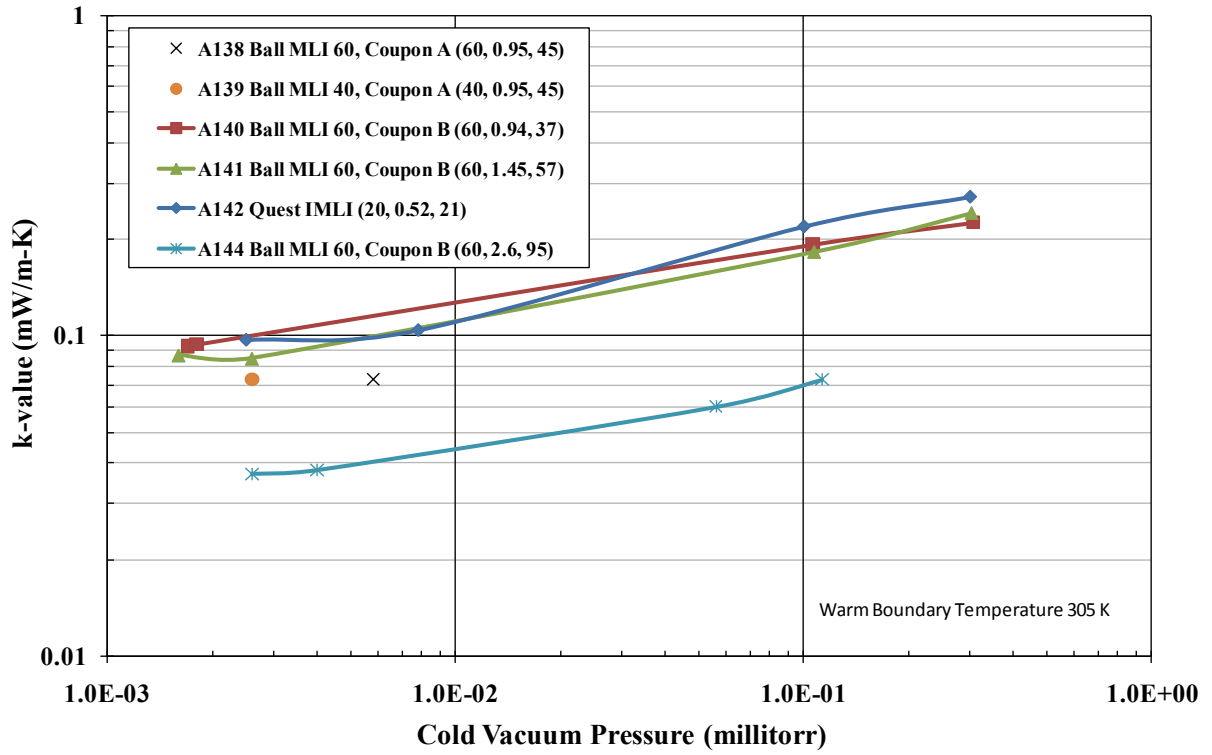


Figure 17: Effective thermal conductivity (k-value) as a function of CVP for MLI systems at a WBT of 305 K

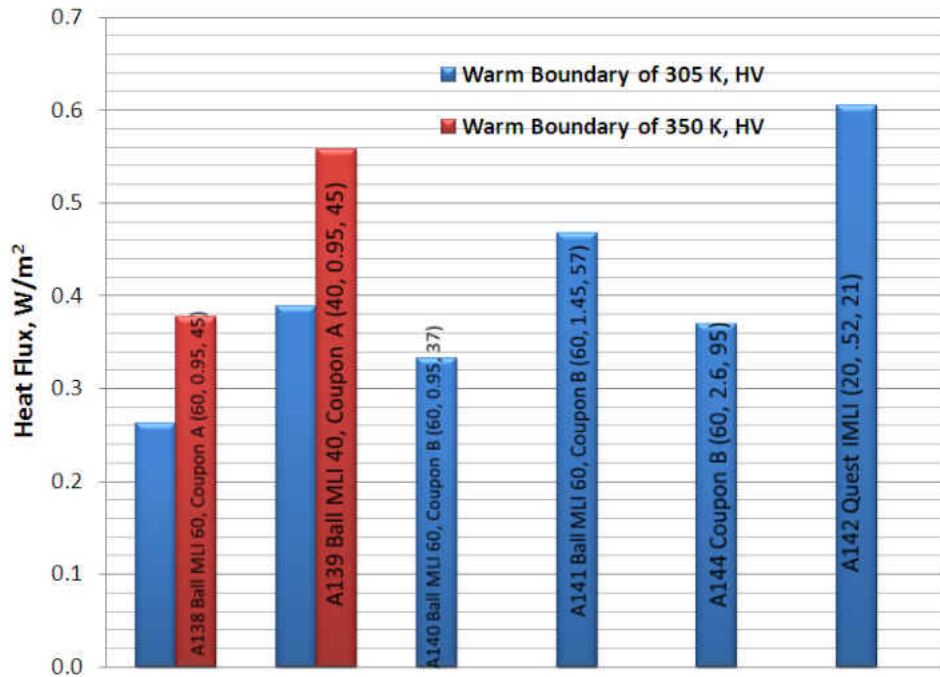


Figure 18: High vacuum heat flux for various MLI systems

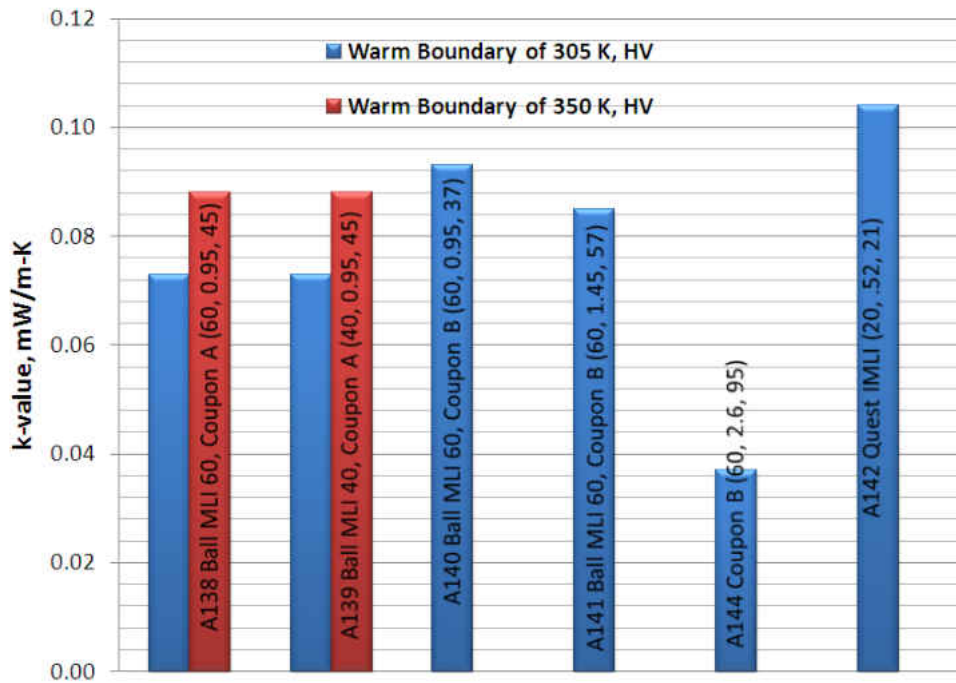


Figure 19: High vacuum effective thermal conductivity (k-value) for various MLI systems

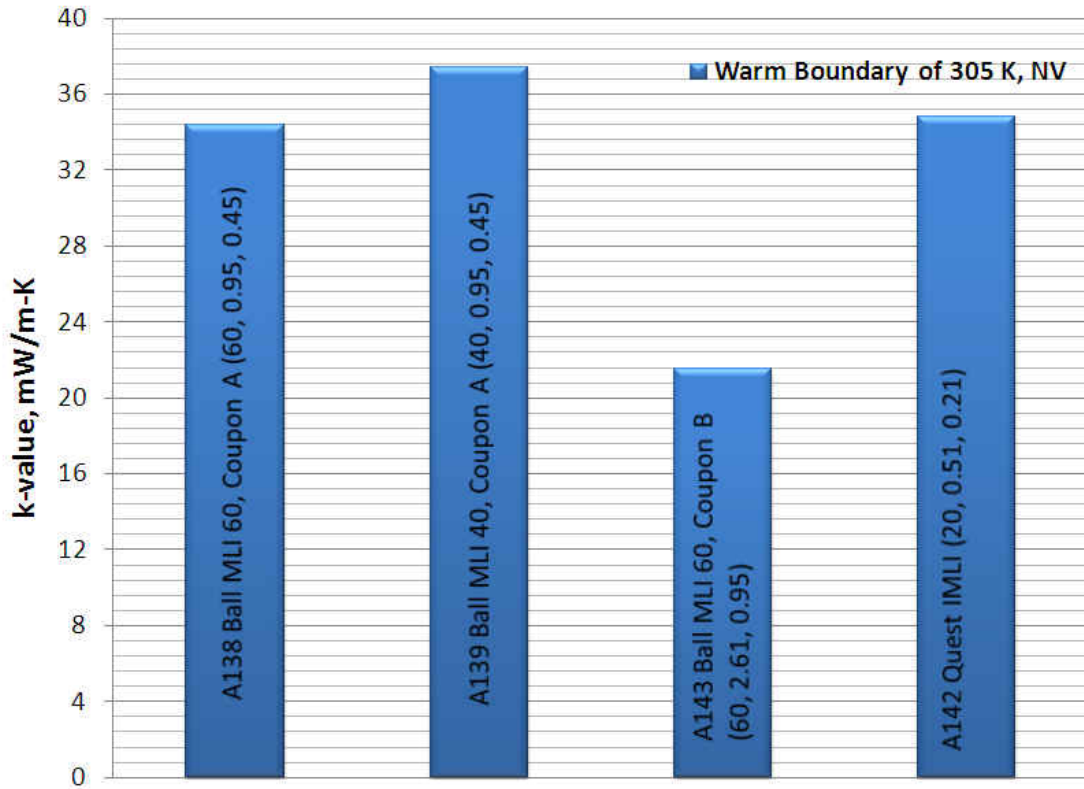


Figure 20: No vacuum k-value test results for various MLI system testing.

Discussion

There are several different pressure regimes that must be considered in the analysis of MLI blankets. The first of these regimes is High Vacuum (HV). For many powder insulations, the heat transfer stops decreasing in the pressure range below 1 millitorr (10^{-3} torr). However, due to the relatively large gaps between the layers, MLI heat transfer does not reach its minimum until 0.001 millitorr (10^{-6} torr). This vacuum pressure level is well into the range of Knudsen numbers (Kn) less than 10^{-4} . The second, most difficult, and least studied regime is Soft

Vacuum (SV). Generally considered at approximately 100 millitorr, SV realistically spans the gap between high vacuum and the transition to continuum flow (roughly 1 millitorr to 1 torr, the linear portion of the thermal conductivity curve). The third regime is No Vacuum (NV) which is the range between about 10 torr and atmospheric pressure (defined as 760 torr at sea-level). For MLI, the heat transfer is generally dominated by gas conduction and convection in this regime and rather constant, yielding the upper plateau in the general thermal performance curve.

Performance at High Vacuum

The tricky part of analyzing or predicting the MLI performance at high vacuum involves picking the correct equation to use. Even though many different spacer materials and perforation combinations were tested, the exact combinations were often times not actually used. Many companies use the traditional equations developed by Keller and Cunningham, traditionally referred to as the “Lockheed equations” (LE) [17]. Additionally, Hastings and Hedayat developed a “Modified Lockheed equation” (MLE) for Dacron netting spacers and a specific perforation pattern that was tested at Marshall Space Flight Center [30]. Even though Fredrickson did some flat plate calorimeter testing of double aluminized mylar and several different types of Dacron netting, no analytical equations was developed [12]. A third equation (New) can be derived from a combination of the two, using the Dacron netting portion of the MLE and the radiation and gas conduction portions of the Lockheed Equation (see equation (26)). The LE and MLE equations are compared to the actual test results at high vacuum in Table 7. The scale factors (SF), or percent error divided by 100, for the 350 K warm boundary test are much lower than the scale factors for the 305 K warm boundary tests, indicating that the

temperature dependence of the equations is not entirely correct. A simple comparison of the temperature power factors of the Lockheed equation gives a number of roughly 4.3, whereas the tested power factor was 2.7 (the power factor theory is displayed in equation (27)). The variance in power factor suggests that conduction is much more of a factor than allowed by the Lockheed equations. Power factors for the same equations (plus the McIntosh method) are shown in Table 8. Care must be taken in applying these equations to the Quest IMLI blanket (A142) due to the different spacer approach of the system.

Table 7: Correlation Comparisons to Test Results

Test/WBT	Test Q (W/m ²)	LE Q (W/m ²)	LE SF	MLE Q (W/m ²)	MLE SF	New Q (W/m ²)	New Q SF
A138/305	0.262	0.144	1.83	0.156	1.68	0.170	1.54
A138/350	0.377	0.258	1.46	0.261	1.44	0.288	1.31
A139/305	0.388	0.206	1.88	0.224	1.73	0.246	1.58
A139/350	0.557	0.374	1.49	0.376	1.48	0.419	1.33
A140/305	0.332	0.136	2.45	0.148	2.24	0.162	2.05
A141/305	0.472	0.176	2.68	0.244	1.94	0.259	1.82
A142/305	0.567	0.364	1.56	0.330	1.72	0.379	1.49
A142/293	0.410	0.292	1.41	0.266	1.54	0.306	1.34
A143/293	0.366	0.148	2.47	0.209	1.75	0.222	1.65
A144/305	0.369	0.388	0.95	0.756	0.49	0.788	0.47

Further investigating Table 7, it can be seen that there is a sharp increase between identical tests of Coupon A (A138) and Coupon B (A140). This result is due to the seaming method discussed in the Experimental Setup section. Even though great care was taken with Coupon B to minimize the tape conduction, the seams contributed 0.13 W/m more heat leak in A140 than A138. Additionally, a previous test series of 40 layers of DAM and Dacron netting was performed at the Cryogenics Test Laboratory., However, in this case each layer was applied

individually (i.e. no sub-blankets). The heat flux for 40 layers at 2.6 layer/mm was 0.398 W/m²; scaling to 60 layers to compare to A144 (0.369 W/m²), a heat flux of 0.265 W/m² is calculated. This result would give a heat load penalty of 0.19 W/m of seam between a continuous rolled MLI blanket and the Coupon B version of testing. Subtracting the two yields a 0.06 W/m seam penalty for Ball's Coupon A seaming technique using sub-blankets of 4 layers Velcro-ed together.

$$\frac{Q}{A} = \frac{\left(2.4E-4 * \left(0.017 + 7E-6 * (800 - T_{avg}) + 2.28e-2 * \ln(T_{avg})\right)\right) \bar{N}^{2.63} (T_h - T_c)}{Ns + 1} + \frac{5.39E-10 * \epsilon * (T_h^{4.67} - T_c^{4.67})}{Ns} + \frac{1.46E4 * P * (T_h^{0.52} - T_c^{0.52})}{Ns} \quad (26)$$

$$\frac{q_{350}}{q_{305}} = \left(\frac{T_{h,350}}{T_{h,305}}\right)^{PF} \quad (27)$$

Additionally, McIntosh developed a physics-based set of equations that includes terms for radiation, solid conduction, and gaseous conduction (or molecular conduction) [2]. Analysis by the author indicates that this is a rather accurate model, but needs an additional term to account for the contact resistance. Bapat did try to develop such a term; however it became extremely complex very quickly, and was only usable for certain materials [52]. In general contact resistance is hard to model a priori; this causes a need for analytical curve fitting or empirical postulating within MLI systems. However, looking at the Temperature Power Factor (shown in Table 8), the McIntosh approach has a much closer PF to reality than either of the empirical equations.

Table 8: Power Factors of and Optimal Layer Densities Various MLI Equations

Equation	Temperature Power Factor (1 layer/mm)	Optimal Layer Density (305 K)	Optimal Layer Density (350 K)
Lockheed	4.30	1.44	1.63
Modified Lockheed	3.65	1.06	1.25
New Q	3.71	1.09	1.29
McIntosh	2.84	N/A	N/A
Actual Test Data	2.7	1.5 - 2.6	----

Three of the tests of three different layer densities were performed at nearly the same thickness. Test articles A139 (40 layers, 0.94 layer/mm), A141 (60 layers, 1.45 layer/mm), and A142 (20 layers, 0.52 layer/mm) were all tested at roughly 40 mm of total blanket thickness. This set of data allows for a direct comparison among tests, with the exception of modifying A141 to account for the change from coupon A to coupon B. Comparative results from these three tests are shown in Table 9. The flux-density product is shown as a hybrid mass and thermal performance property and comparison metric. These comparisons show that while the lower the density (at a constant thickness) and the higher the heat flux, the areal density decreases much quicker than the heat flux increases. Figure 21 shows graphically the test data for Coupon B, in a similar manner as Figure 6 shows the theoretical data. The mass curve looks about as predicted; however, the thermal conductivity curve does not show an optimal layer density probably due to the limiting upper layer density that was tested. These data combined with test data at higher layer densities (see Figure 22) suggest an optimal layer density between

1.5 and 2.6 layers/mm. However, in terms of the combination of mass and heat transfer, the optimal layer density appears to be as low as reasonably possible.

Table 9: Effect of Layer Density on Heat Flux and Mass

	A141 60 layers 1.45 layer/mm	A139 40 layers 0.94 layer/mm	A142 20 layers 0.52 layer/mm
Heat Flux (W/m ²)	0.367	0.388	0.567
Mass (gram)	1565	1265	526
Areal Density (kg/m ²)	4.18	3.35	1.42
Flux Density Product (W·kg/m ⁴)	1.53	1.30	0.81

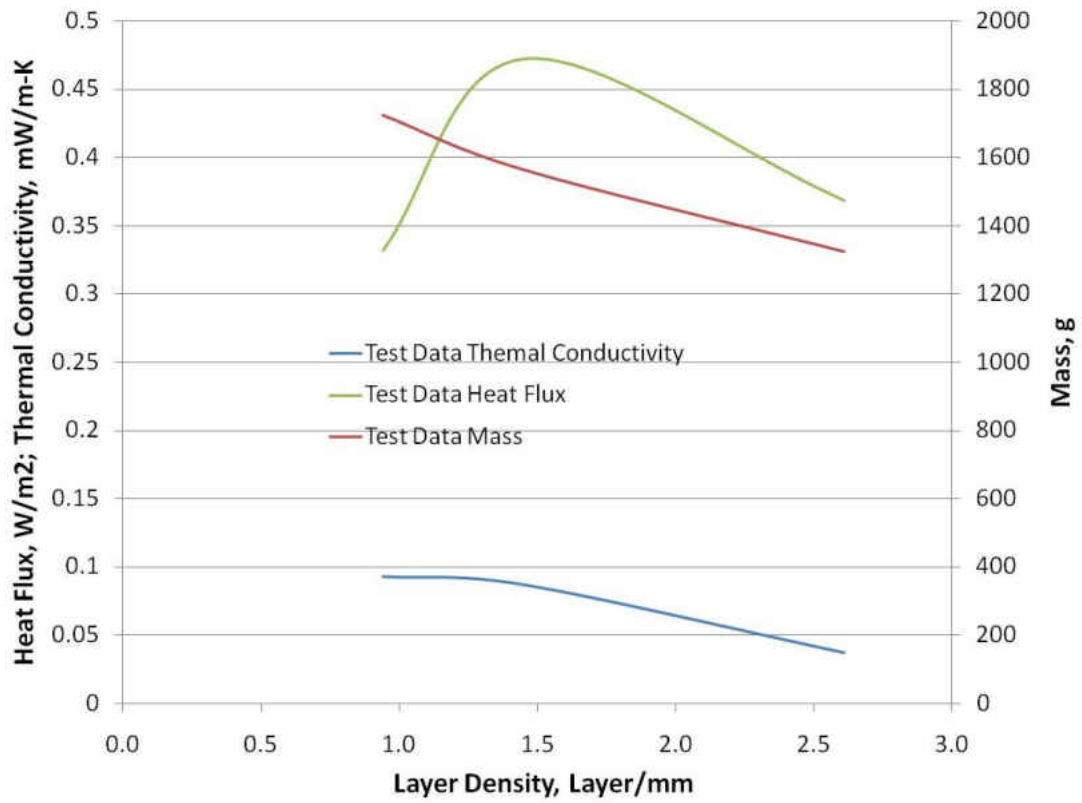


Figure 21: Test data as function of layer density

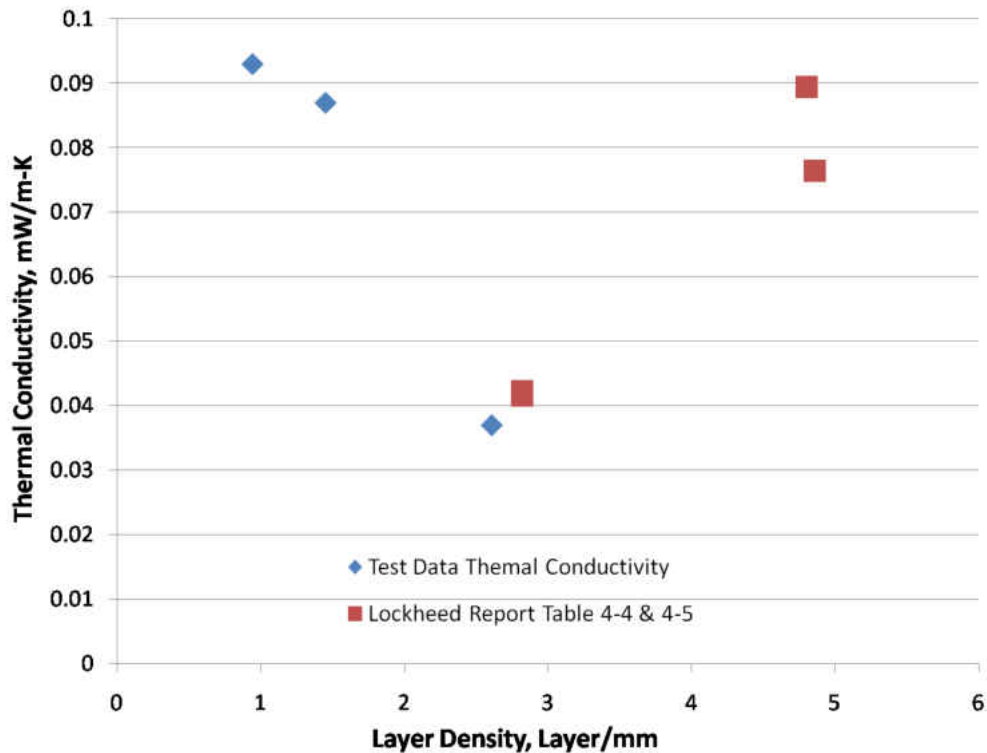


Figure 22: Thermal conductivity test data plotted as a function of layer density

Performance at Degraded and No Vacuum

Almost no analytical work has been done in the soft vacuum regime. The transition between the continuum and free molecular flow regimes is complicated. Gu attempted to curve fit data from Fesmire and Augustynowicz using a double logistical dose response equation [53]. The author's attempts to recreate this equation have yielded different results than the published work. The development of a new pressure fitting equation to match this region is discussed in the Modification of McIntosh Model section. For many cases, such as loss of vacuum in transfer lines, a good understanding of the degraded vacuum properties are needed in order to do

understand the implications of these failures to the safety of the entire system. Fesmire [43] and Sun [40] have previously performed testing, but did not attempt to model the results.

Test results of MLI at no vacuum have shown that the thermal performance is closely linked to the performance of the interstitial gas. However, this has not previously been done with low density MLI. Comparing the results of the blankets that were tested at ambient pressure reveals that there is a sharp break between the low density and medium to high density blankets (see Figure 20). These data also suggest that the thickness of the blanket is not the prime suspect as A139 and A143 were the same thickness. Apparently the wide spaces between the layers allow for natural convection in the vertical positioning and thus the convection increases the total heat transfer through the blanket. This effect is further suggested when examining the temperature profile of the A138 at no vacuum and comparing to the typical no vacuum temperature profile (Figure 23). The temperature gradient is much steeper close to the cold mass than it is further from the cold mass, indicating that heat is being transferred in some other fashion.

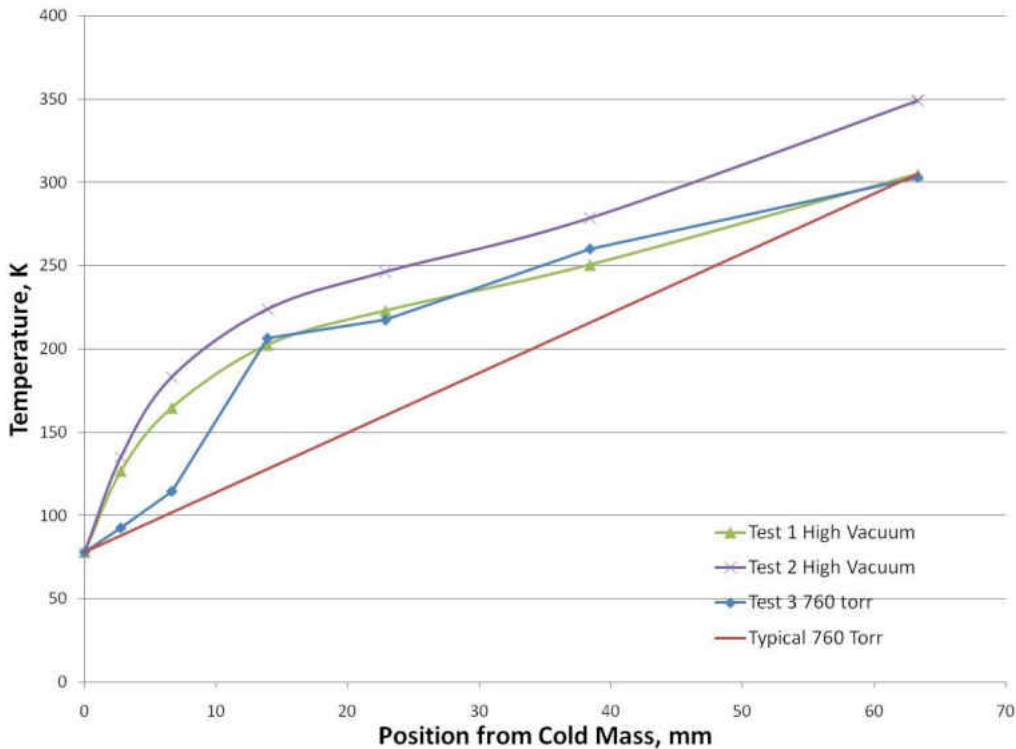


Figure 23: Temperature profiles for test series A138.

Modification of McIntosh Model for all Pressure Regimes

In order to account for the various pressure regimes, a modified McIntosh layer by layer model was developed. In a similar fashion as Gu, a pressure coefficient was added to the pressure term from the original equations [53]. At high vacuum, this term approaches 1 and at soft vacuum and high vacuum, the term forces the gas conduction to dominate the heat transfer. However, comparing the test results with several historical data series from the Cryogenics Test Laboratory as a function of cold vacuum pressure showed some interesting variations (see Figure 24). The transition between high vacuum to soft vacuum appears to change with layer density. This observation is most notable with the 0.5 layer/mm Quest blanket, however, each of the varying densities does slowly change the transition point at higher pressures. This effect leads to

soft vacuum performance variations by as much as an order of magnitude depending on the layer density. The conclusion that can be drawn from this is two-fold: first, those MLI systems with lower layer densities need a lower pressure to achieve the ultimate performance, and secondly, that gas conduction at high vacuum is not a function of pressure as suggested by Corruccini, but a function of something else.

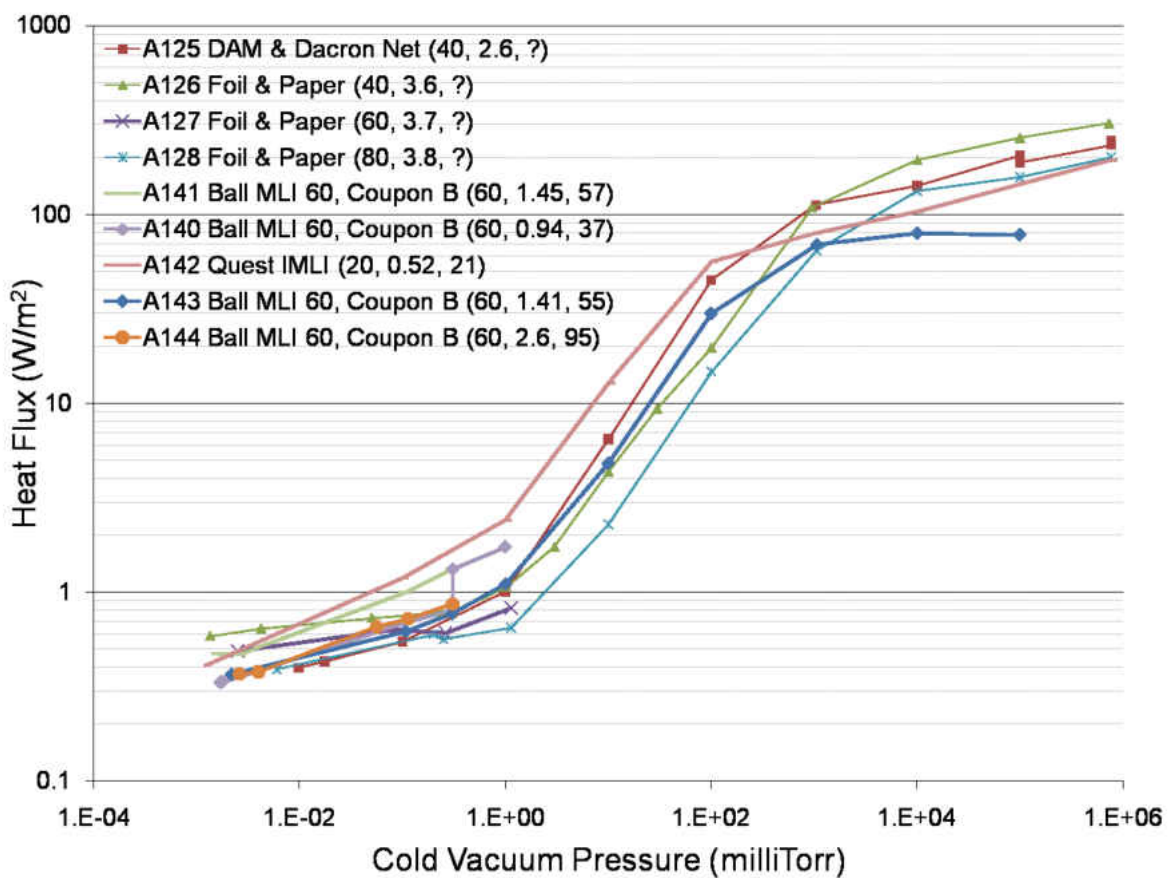


Figure 24: Heat Flux vs CVP for several MLI systems

Further investigation suggested that the heat flux is a function of inverse Knudsen number as opposed to pressure (see Figure 25). The Knudsen number is a non-dimensional

number that compares the mean free path of a gas to the geometry containing that gas. The mean free path of the gas (λ) can be found by:

$$\lambda = \frac{k_B T}{\xi^2 P} \quad (28)$$

Thus the Knudsen number (Kn) is:

$$Kn = \frac{\lambda}{N/\bar{N}} \quad (29)$$

And the inverse Knudsen number (iKn) is:

$$iKn = \frac{N}{\bar{N}\lambda} \quad (30)$$

In adapting this new relationship to the McIntosh set of equations, a new term must be added to account for the Knudsen number relationship instead of the pressure relationship. The original term for gas conduction was first derived by Corruccini [54]

$$H = \left(\frac{\gamma+1}{\gamma-1} \sqrt{\frac{R}{8\pi MT}} \right) \alpha P (T_h - T_c) \quad (31)$$

This is turned into conductivity by McIntosh [2] such that:

$$h = \left(\frac{\gamma+1}{\gamma-1} \sqrt{\frac{R}{8\pi MT}} \right) \alpha P \quad (32)$$

The pressure coefficient is then added such that:

$$h = \left(\frac{\gamma+1}{\gamma-1} \sqrt{\frac{R}{8\pi MT}} \right) \alpha Z \quad (33)$$

where:

$$Z(Kn) = q''_{low} \left(\frac{q''_{high}}{q''_{low}} \right)^{\frac{1}{(1+Kn/b)^\delta}} \quad (34)$$

Such that:

$$q''_{\text{low}} = 0.07$$

$$q''_{\text{high}} = 60$$

$$k_0 = 1.8$$

$$\delta = 0.5$$

Each of the variables has a purpose q''_{low} quantitative represents the heat flux at high vacuum, q''_{high} is a quantitative representative of the heat flux at no vacuum, k_0 controls the shift of the transition as a function of inverse Knudsen number, and δ controls the curvature of the two ends as they flow into the diagonal of the function. The result of applying these correction factors is shown in Figure 25 as the Johnson fit. This curve fit allows the determination of the thermal performance of MLI blankets on a layer by layer basis throughout the entire vacuum regime.

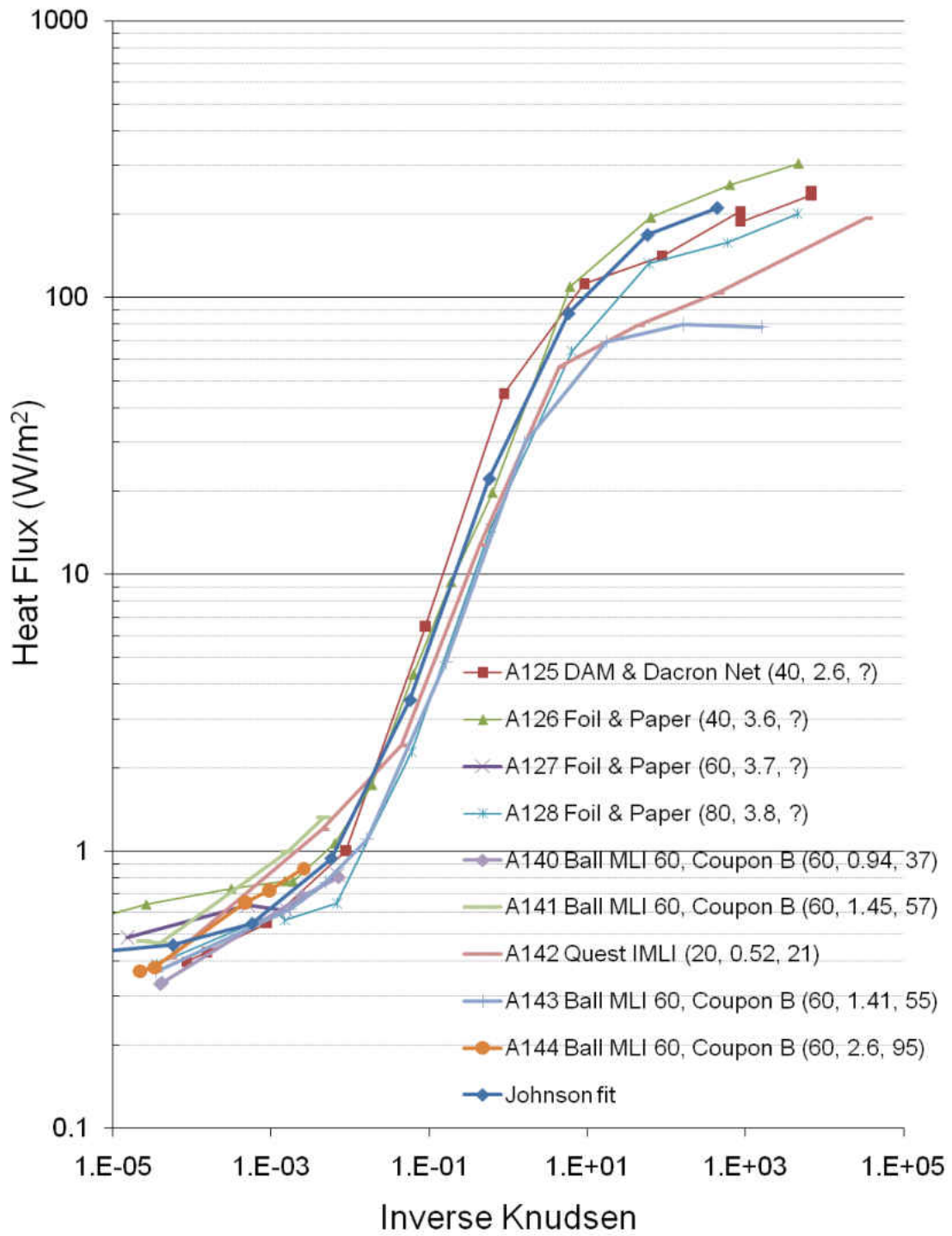


Figure 25: Heat Flux as a Function of Inverse Knudsen Number for Several MLI Systems

CHAPTER FIVE: CONCLUSIONS

Several MLI systems were tested on a boil-off calorimeter at the Kennedy Space Center. These tests allowed for the following variables: layer density, warm boundary temperature, vacuum level, and number of layers. Existing analytical expressions for determining heat flux over a wide range for each of these variables were compared to the test results.

MLI was tested at low layer densities. The performance at lower layer densities was shown to vary by over 100% from the predicted performance using existing solution methods. However, a new solution method was generated that greatly reduced the error down to 40%.

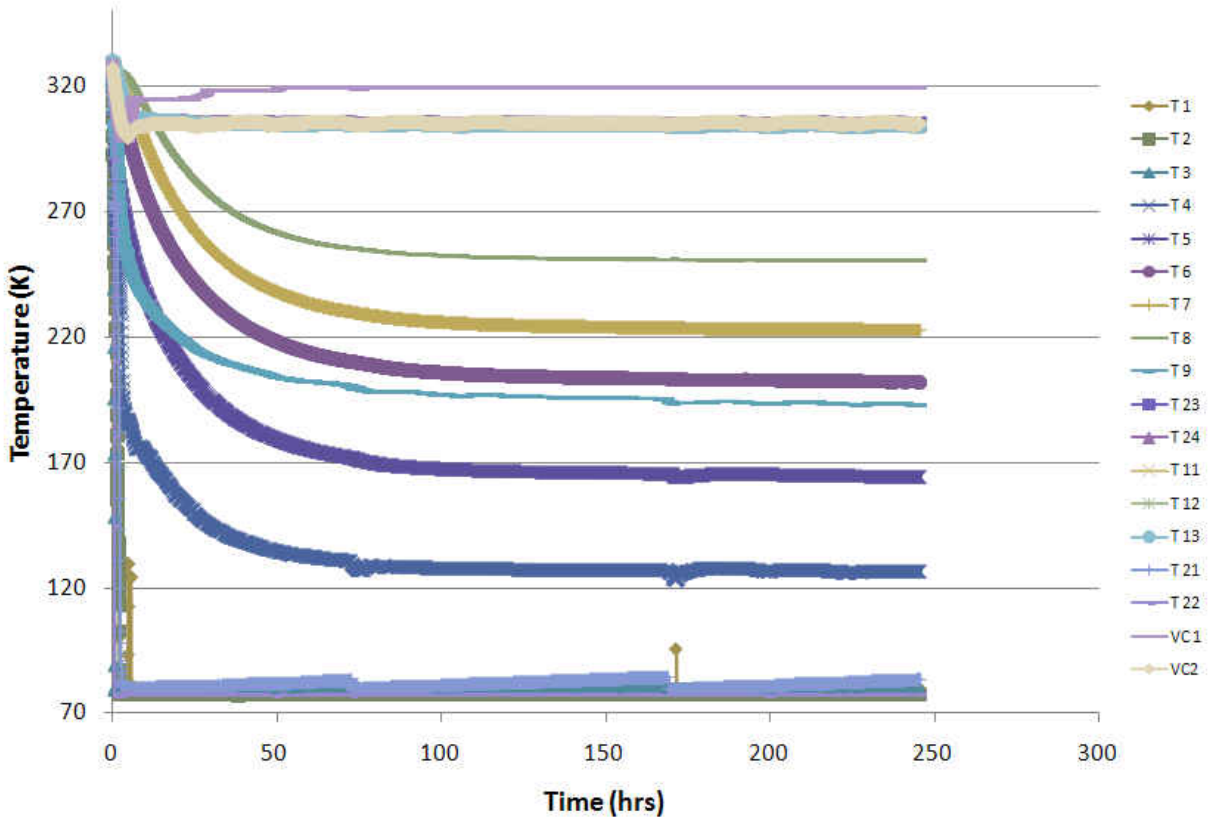
An analytical solution for the optimal layer density of MLI systems was derived and compared to the test data. Several modifications were suggested to more closely predict the performance of such MLI systems. The test data indicate that the power factor of the equations should be lower than it is in most equations. The optimal layer density for boundary temperatures of 77 K and 305 K was shown to be between 1.5 and 2.6 layers/mm, closer to the later. This value is much higher than the analytically predicted values between 1.0 and 1.5 layer/mm. This suggests that radiation is more important in determining this optimal layer density than the equations let on.

MLI heat transfer was shown to be a function of inverse Knudsen number as opposed to strictly cold vacuum pressure. An analytical solution for MLI performance as a function of inverse Knudsen number was obtained using a layer-by-layer analysis. This solution passes through all pressure regimes from high vacuum to soft vacuum to no vacuum. This solution implies that MLI systems with lower layer densities need a lower pressure to achieve the

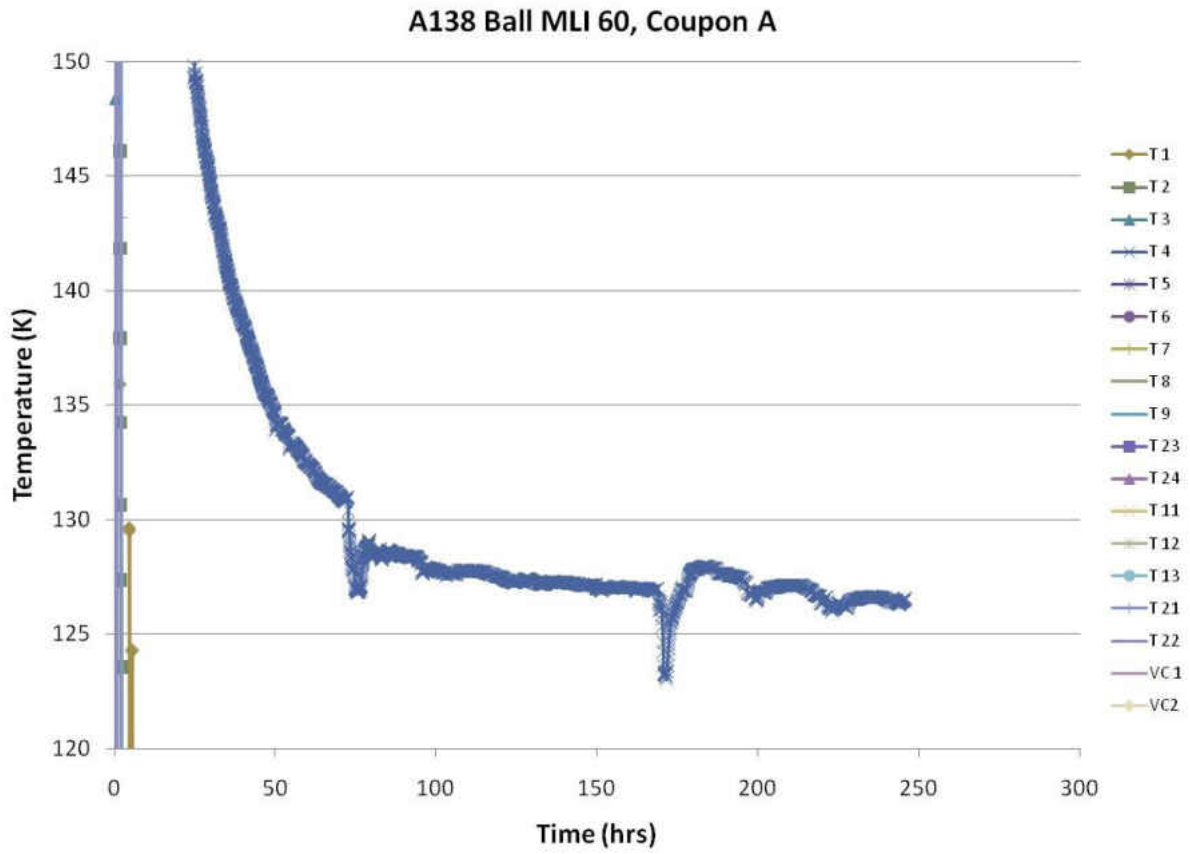
ultimate performance and that gas conduction at high vacuum is not strictly a function of pressure as suggested by Corruccini, but a function of the Knudsen number.

APPENDIX: VARIOUS DATA PLOTS FROM TESTING

A138 Ball MLI 60, Coupon A

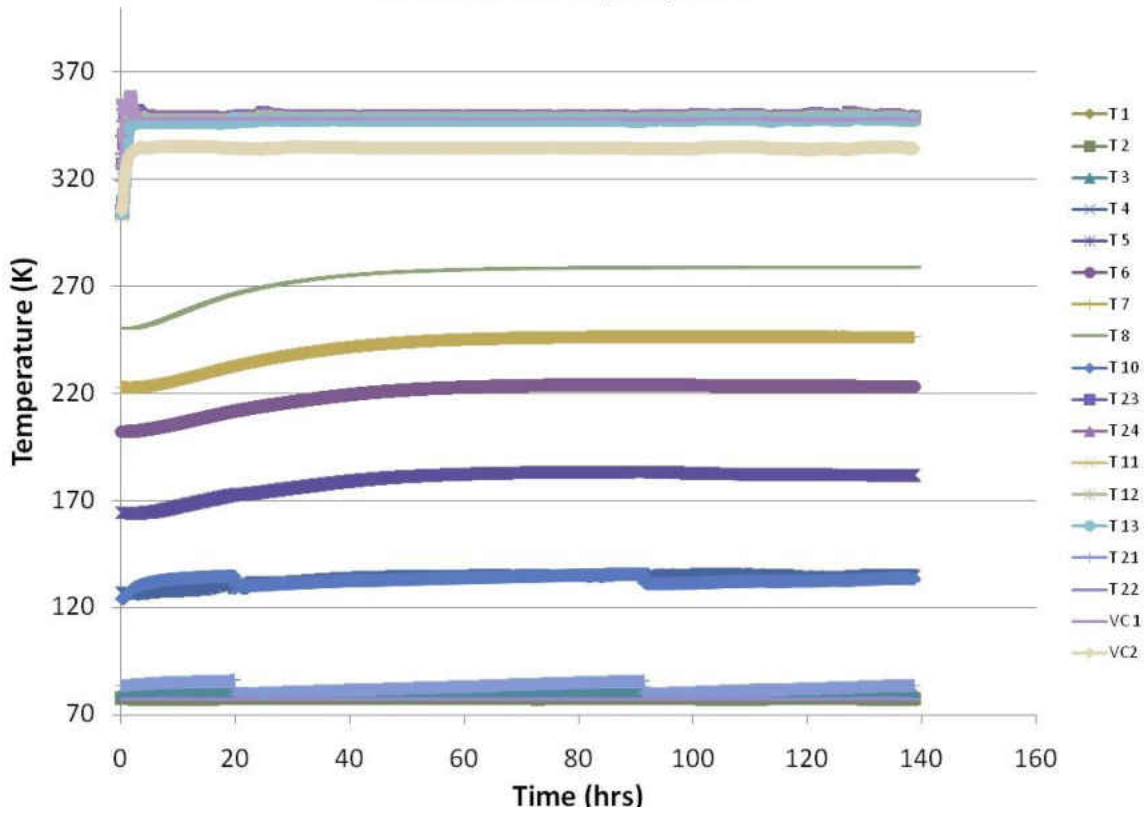


Typical temperature profile for entire blanket coming to steady state at high vacuum for first 250 hours

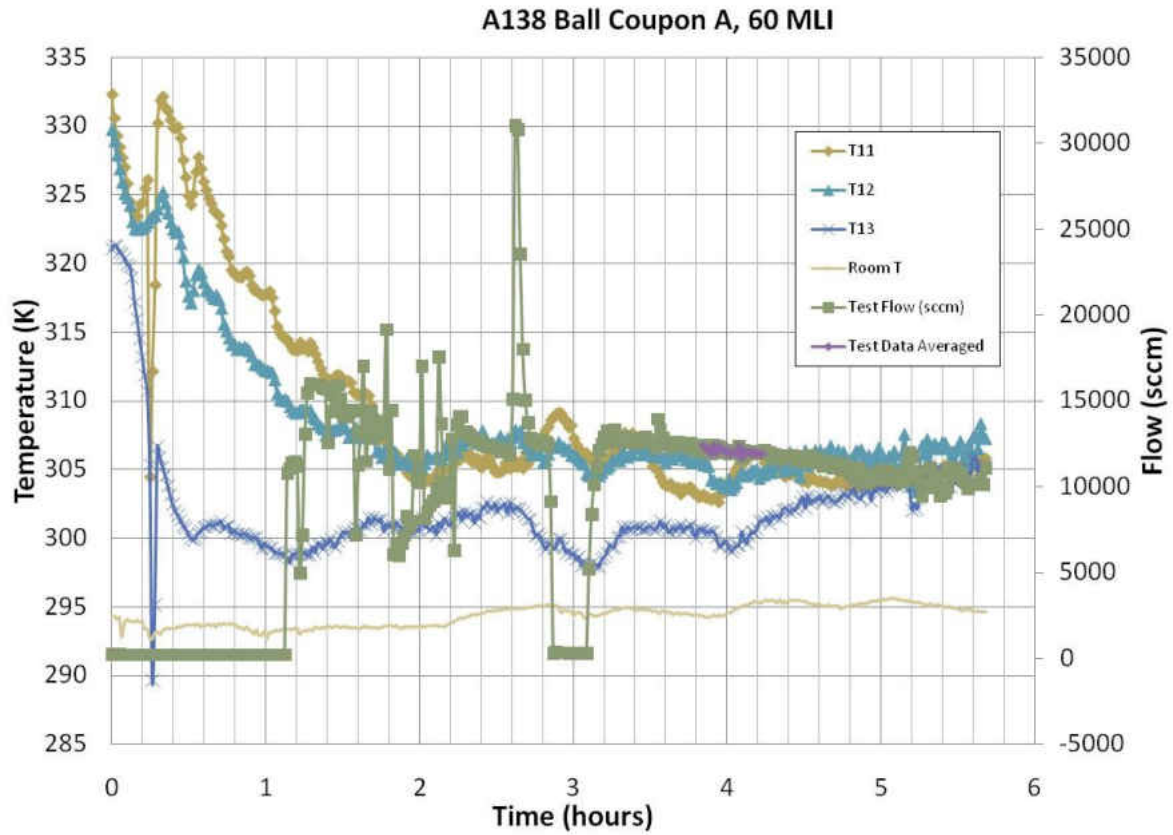


T4 (sub-blanket 1) for first 250 hours of testing, eventually coming to steady state at high vacuum

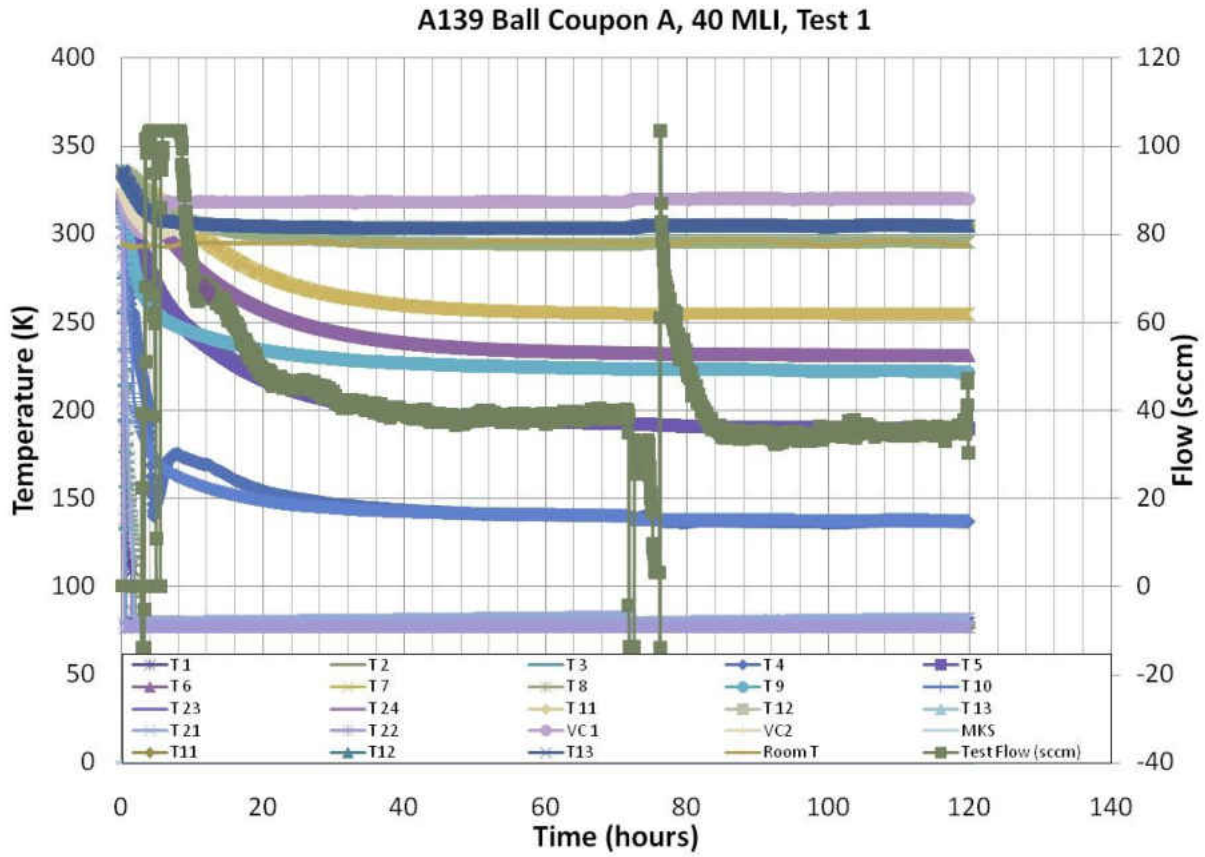
A138 Ball MLI 60, Coupon A



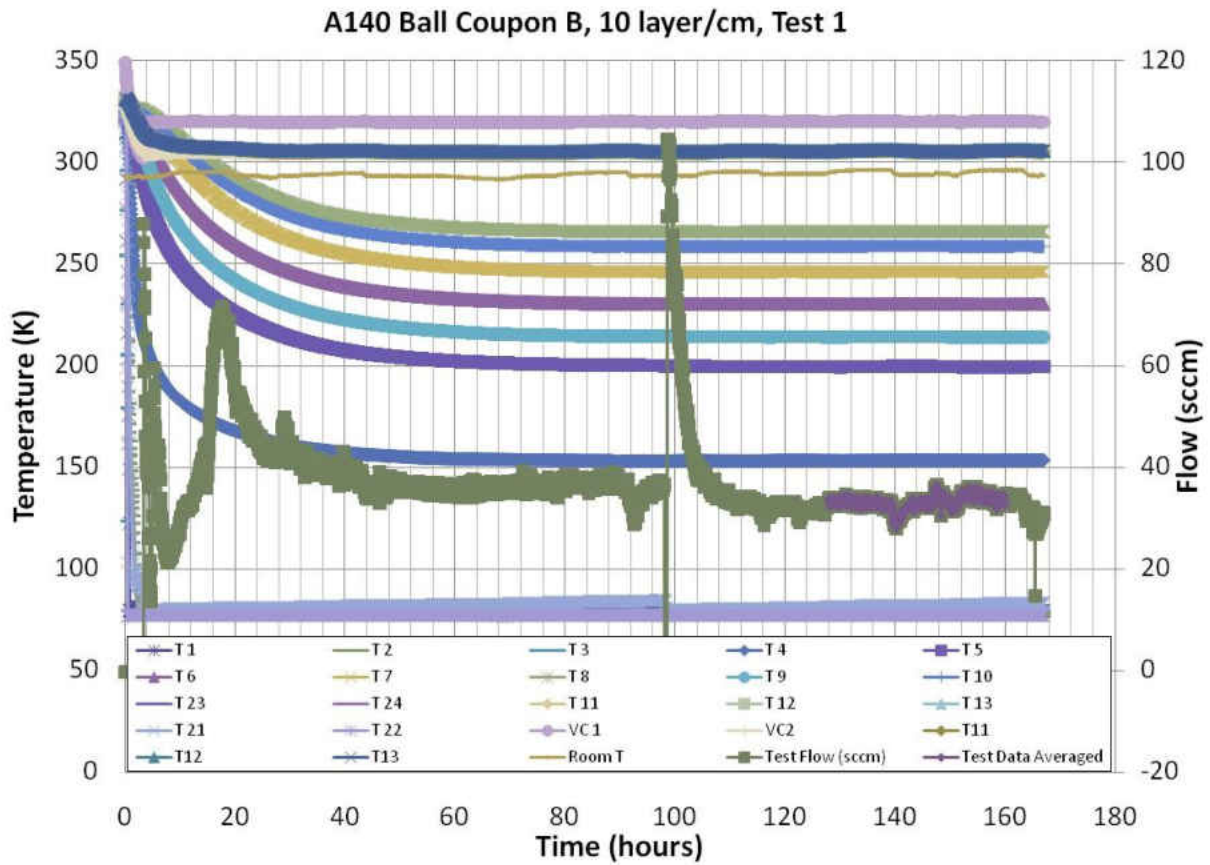
Typical Temperature profile approaching steady state at 350 K warm boundary temperature following a 305 K warm boundary temperature test



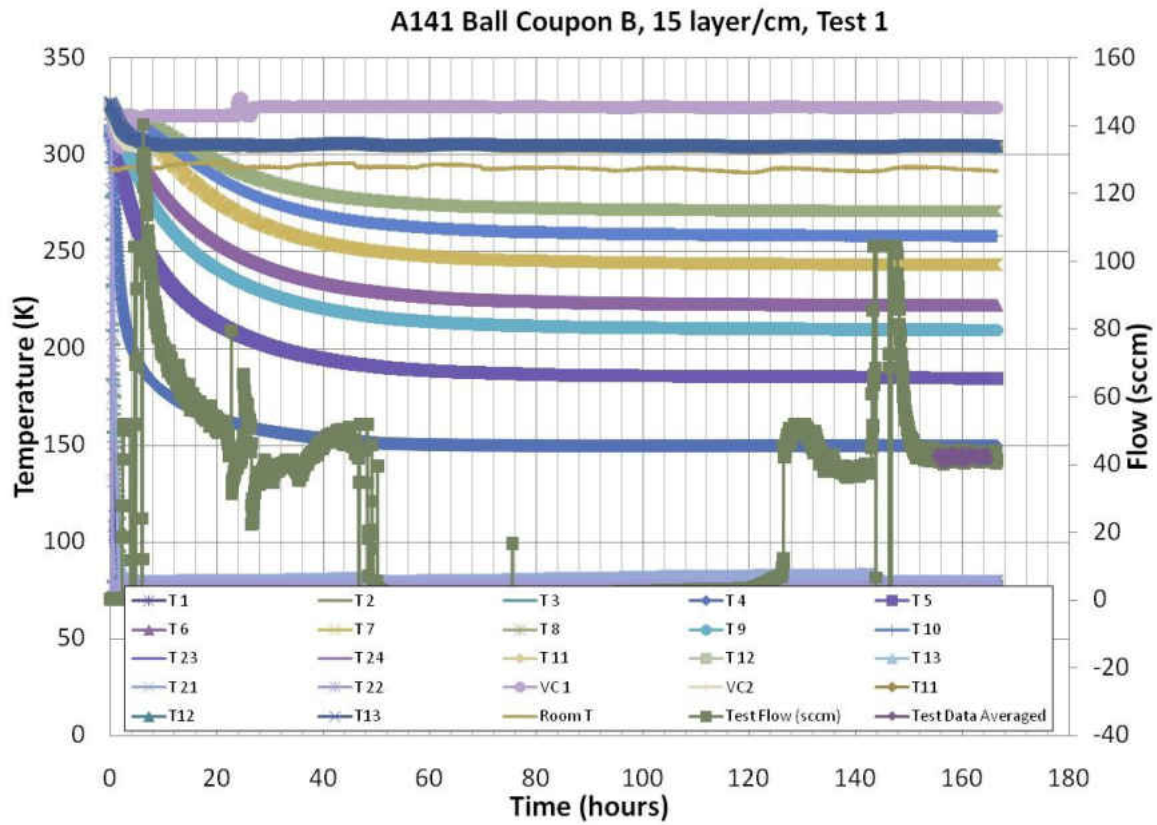
Typical no-vacuum test boil-off flow and warm boundary temperature, data averaged between 92 and 88 % full per internal testing standards.



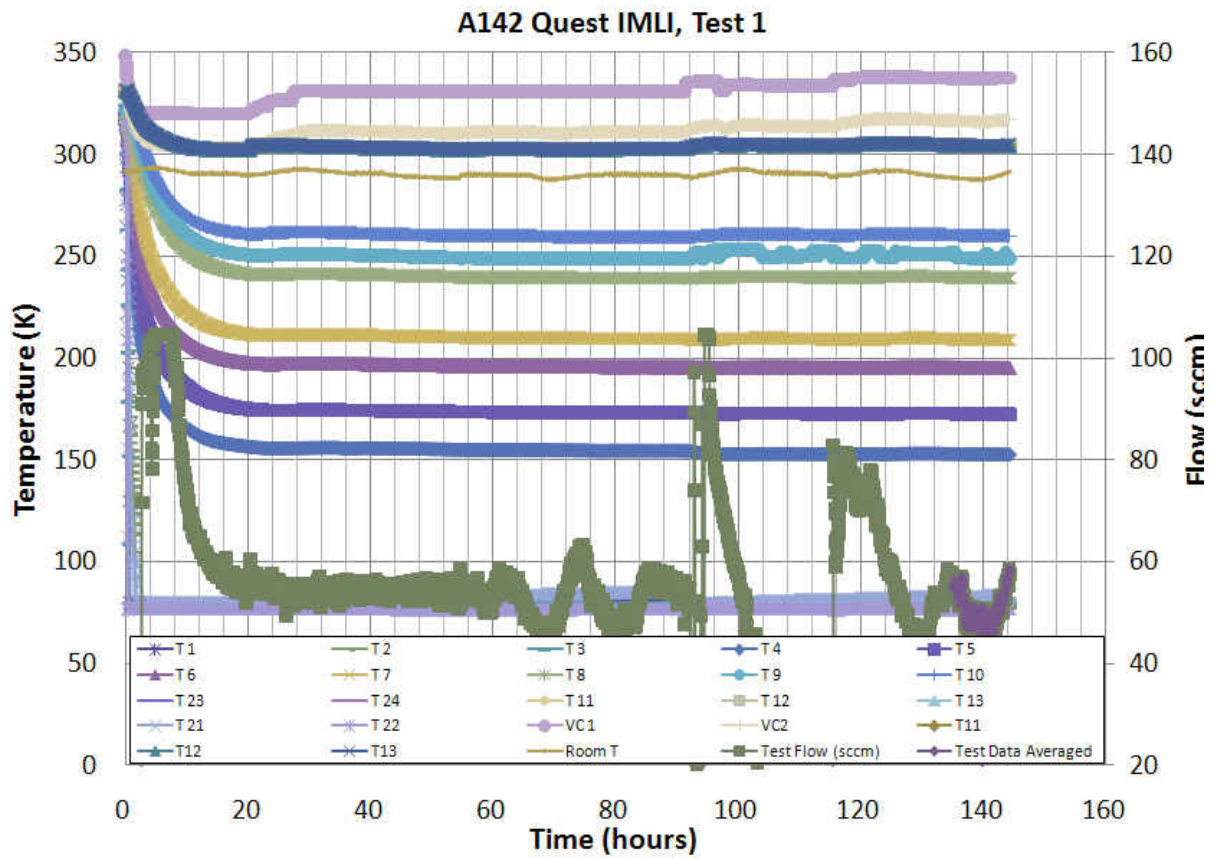
High Vacuum test shows repeatability after refill and cool down duration for only 40 layers.



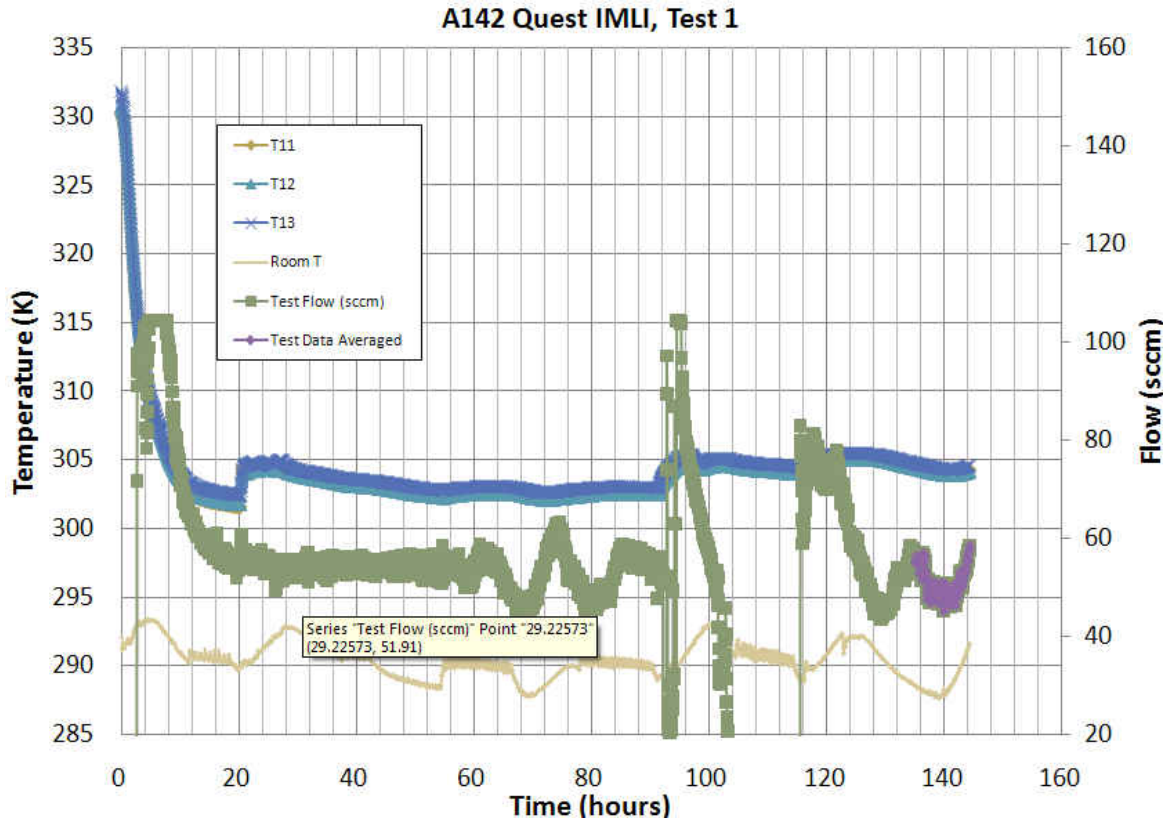
Coupon B high vacuum test, doesn't takes over 100 hours just to chill MLI to steady state



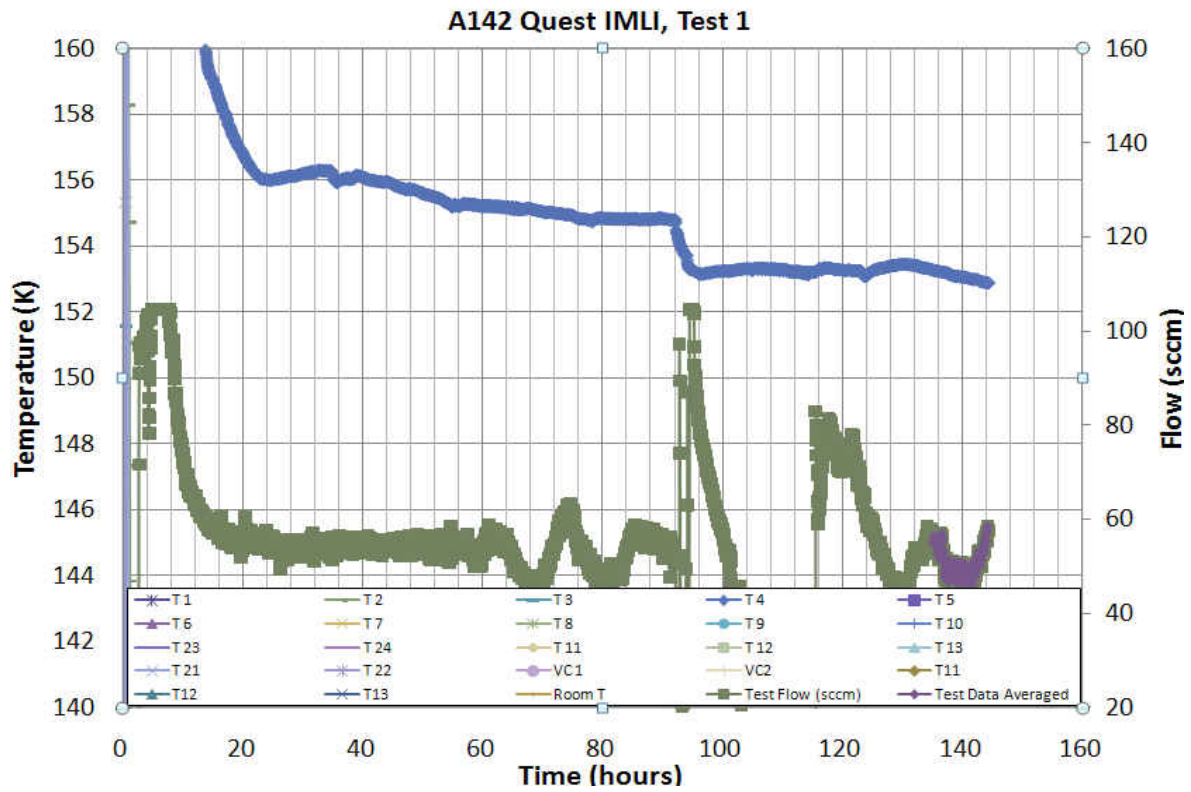
Due to improper conditioning (too high of a back pressure maintained), the flow went to zero as the liquid in the test chamber warmed up to the new test pressure (this was approximately 5 torr – 70 Pa – of differential pressure applied on liquid).



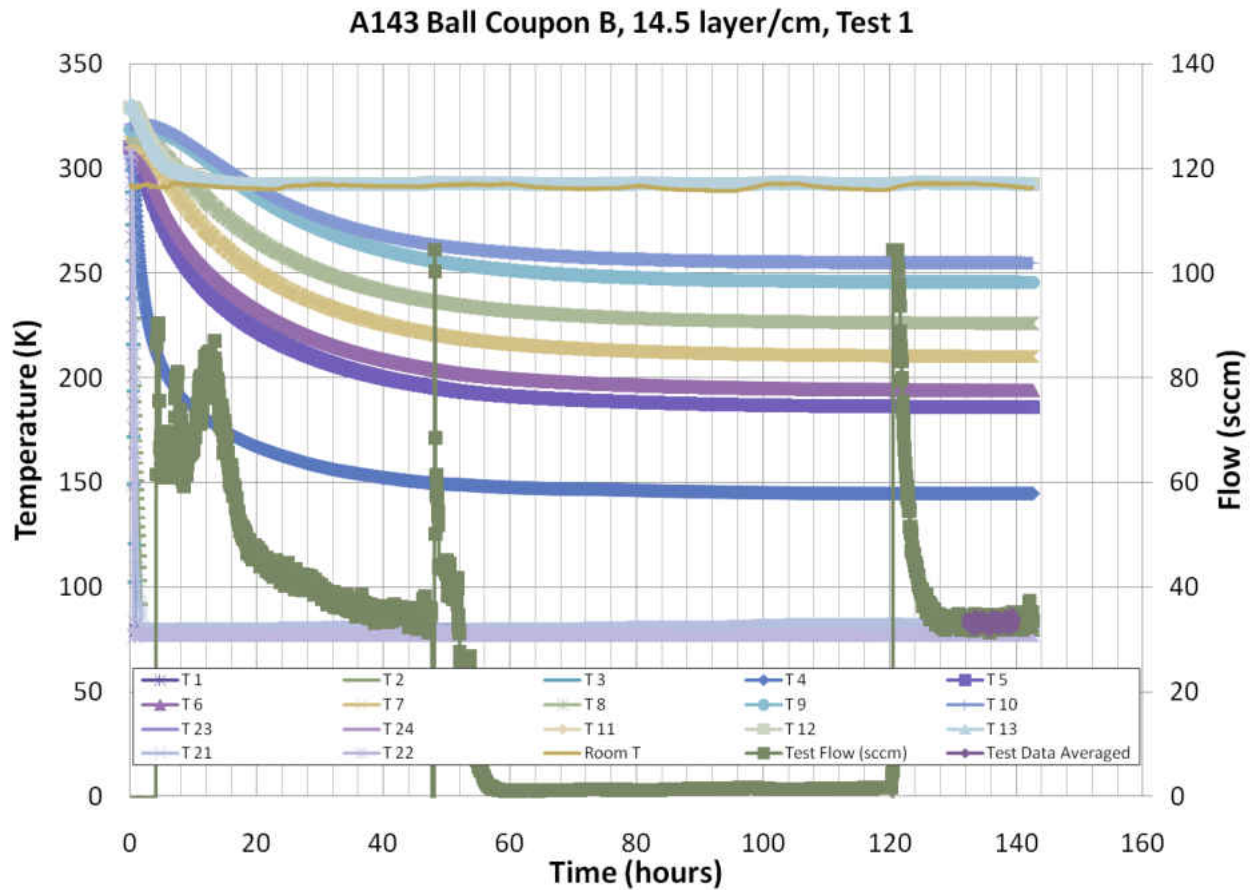
Notice loss of back-pressure control during this test at approximately 60 hours.



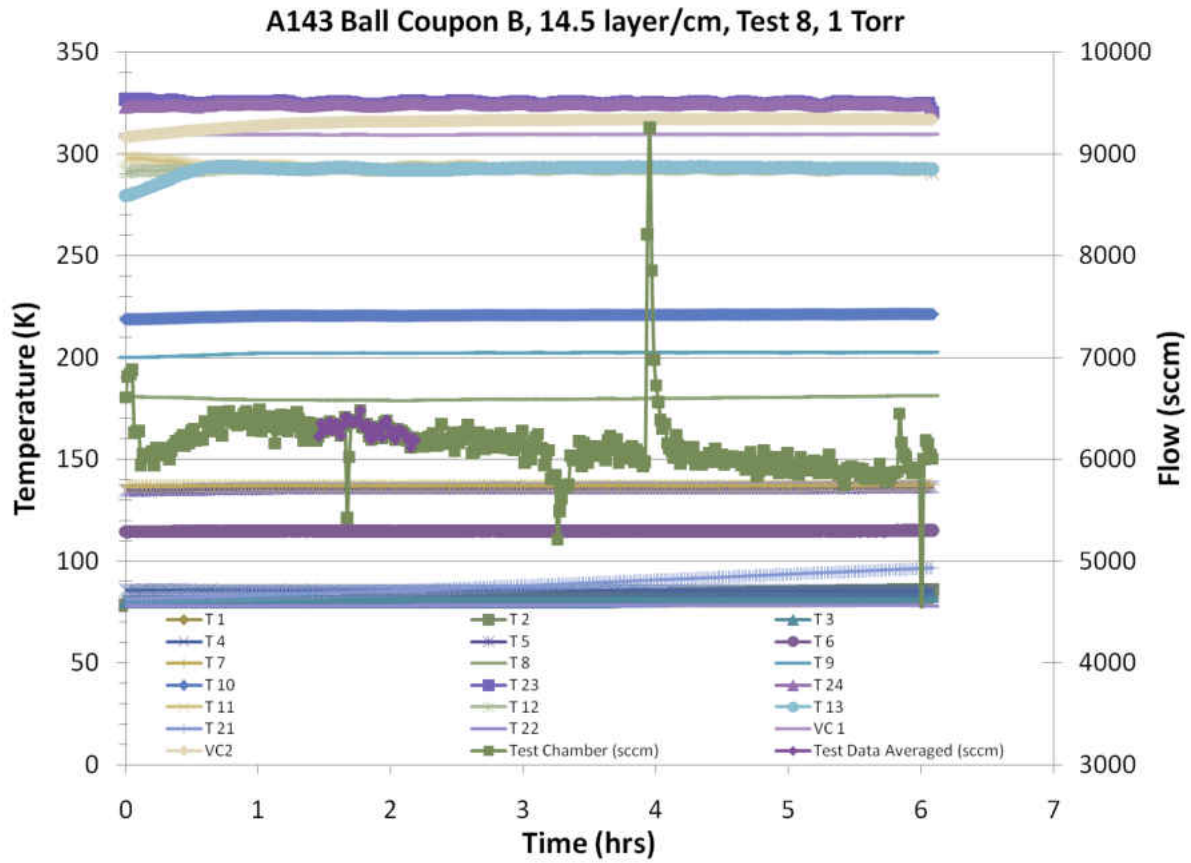
Again, loss of back pressure control shown with variations in room temperature and warm boundary temperature.



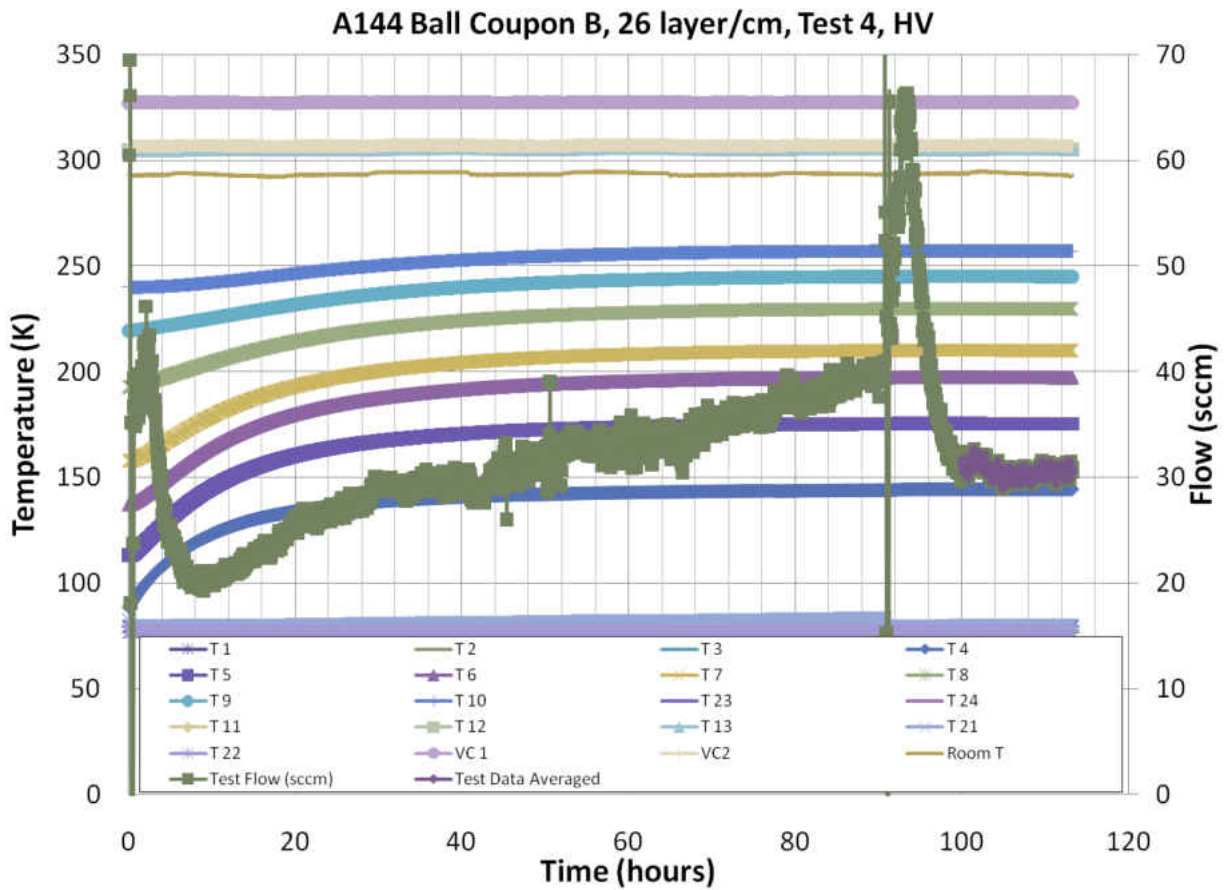
Note: Temperature stability of T4 after a certain length of time. Notice loss of back-pressure control during this test



Note: The period between approximately 56 and 120 hours is the duration that it took the test chamber to acclimate to the several torr backpressure being applied. In this case, as the test was run during a slow time in the lab, more backpressure was applied (several torr) and the time was not as important.



Note: This test was run at 1 Torr (1000 millitorr), the flows are much higher than previous tests and the averaged data is between 92 and 88% full per internal test standards.



Note: This test was the second high vacuum test run on A144, it was run after a 0.3 millitorr test, and the change in layer temperature is quite evident in the first 60 hours of the test, a refill at approximately 90 hours helped to steady the test out.

REFERENCES

- [1] R. G. Scurlock, B. Saull, Development of MultiLayer Insulations with Thermal Conductivities Below $0.1\text{mW cm}^{-1}\text{ K}^{-1}$, *Cryogenics* (1976) 303-311.
- [2] G. E. McIntosh, Layer by Layer MLI Calculation using a Separated Mode Equation, in: *Advances in Cryogenic Engineering*, Vol 39B, Plenum Press, NY, 1993, pp. 1683-1690.
- [3] Ralph G. Scurlock, *History and Origins of Cryogenics*, Oxford University Press, NY, 1992.
- [4] W. D. Cornell, Radiation Shield supports in Vacuum Insulated Containers, U.S. Patent No. 2,643,022, 1947.
- [5] I. Black, P. E. Glaser, Progress Report on Development of High-Efficiency Insulation, in: *Advances in Cryogenic Engineering*, Vol. 6, Plenum Press, Inc, NY, 1961, pp. 32-41.
- [6] Basic Investigation of Multi-Layer Insulation Systems, NASA-CR-54191, 1964.
- [7] I. E. Black, P. E. Glaser, Effects of Compressive Loads on the Heat Flux Through Multilayer Insulation, in: *Advances in Cryogenic Engineering*, Vol 11, Plenum Press, NY, 1966, pp. 26-34.
- [8] Advanced Studies on Multilayer Insulation Systems, NASA-CR-72368, 1968.
- [9] P. E. Glaser, Design of Thermal Protection Systems for Liquid Hydrogen Tanks, NASA-CR-62859, 1962.
- [10] R. B. Hinckley, Liquid Propellant Losses During Space Flight, NASA CR-53336, 1964.
- [11] G. O. Fredrickson, M. C. Coes, et al., Ranking and Selection Insulation Systems for MNV Application, Special Report No. 1, Investigation of High-Performance Insulation Application Problems, NASA CR-112337, 1969.

- [12] G. O. Fredrickson, Investigation of High-Performance Insulation Application Problems, Final Report, NASA CR-124400, 1973.
- [13] D. J. Daniels, P. I. Kawano, et al., An Evaluation of Orbital Workshop Passive Thermal Control Surfaces, in: , The American Society of Mechanical Engineers, NY, 1974.
- [14] K. E. Leonard, Cryogenic Insulation Development, Final Report, NASA-CR-123938, 1972.
- [15] A. B. Walburn, Development of a Reusable Flightweight Cryogenic Storage System, AIAA 74-726, 1974.
- [16] G. R. Cunnington, C. W. Keller, et al., Thermal Performance of Multilayer Insulations, Interim Report, LMSC-A903316/NASA CR-72605, Lockheed Missile and Space Company, Sunnyvale, CA, 1971.
- [17] C. W. Keller, G. R. Cunnington, et al., Thermal Performance of Multi-layer Insulations, Final Report, Contract NAS3-14377, Lockheed Missile and Space Company, Sunnyvale, CA, 1974.
- [18] C740M ASTM C740, Standard Practice for Evacuated Reflective Insulation In Cryogenic Service, DOI: 10.1520/C0740_C0740M-97R09, ASTM International, West Conshohocken, PA, 2009.
- [19] G. R. Cunnington, C. L. Tien, A Study of Heat-Transfer Processes in Multilayer Insulations, AIAA 69-607 , 1969.
- [20] C. L. Tien, G. R. Cunnington, Radiation Heat Transfer in Multilayer Insulation Having Perforated Shields, AIAA Paper 73-718, American Institute of Aeronautics and Astronautics, NY, 1973.

- [21] I. E. Spradley, T. C. Nast, et al., Experimental Studies of Multilayer Insulation at Very Low Temperatures, in: Advances in Cryogenic Engineering, Vol. 35A, Plenum Publishers, NY, 1990, pp. 477-486.
- [22] T. C. Nast, A Review of Multilayer Insulation Theory, Calorimeter Measurements, and Applications, in: J. P. Kelley, J. Goodman, (Eds.), Recent Advances in Cryogenic Engineering - 1993, ASME HTD-Vol. 267, American Society of Mechanical Engineers, New York, 1993, pp. 29-43.
- [23] Shuttle Orbiter Discovery (OV-103), Kennedy Space Center Science and Technology, Accessed: June 7, 2010, Published: August 8, 2005, <http://science.ksc.nasa.gov/shuttle/resources/orbiters/discovery.html>.
- [24] R. A. Mohling, H. L. Geir, et al., Multilayer Insulation Thick Blanket Performance Demonstration, AFAL TR-87-037, Ball Aerospace Systems Group, Boulder, CO, July 1987.
- [25] R.A. Mohling, M. J. Bergeland, et al., Multilayer Insulation Thick Blanket Performance Demonstration, AFAL TR-90-005, Ball Aerospace Systems Group, Boulder, Co, April 1990.
- [26] E. H. Hyde, Multilayer Insulation Thermal Protection Systems Technology, Research Achievements IV NASA TM X-64561 (1971) 5-52.
- [27] J. M. Stuckey, Multilayer High Performance Insulation Materials, Research Achievements IV NASA TM X-64561 (1971) 93-98.

- [28] R. J. Stochl, P. J. Dempsy, et al., Variable Density MLI Test Results, in: *Advances in Cryogenic Engineering*, Vol. 41, Plenum Publishers, NY, 1996, pp. 101-107.
- [29] J. J. Martin, L. J. Hastings, Large Scale Liquid Hydrogen Testing of a Variable Density Multilayer Insulation with a Foam Substrate, NASA TM-2001-211089, 2001.
- [30] L. Hastings, A. Hedayat, et al., Analytical Modeling and Test Correlation of Variable Density Multilayer Insulation for Cryogenic Storage, NASA-TM-2004-213175, 2004.
- [31] B. P.M. Helvensteijn, L. J. Salerno, et al., Thermal Conductivity Measurements of Aerogel-Impregnated Shuttle Tile at Cryogenic Temperatures, in: *Advances in Cryogenic Engineering*, Vol 47B, American Institute of Physics, Melville, NY, 2002, pp. 1549-1556.
- [32] R. J. Stochl, M. E. Moran, Multi-Layer Insulation Test Rig for MLI Design Code Validation, AIAA 2007-6186, 2007.
- [33] I. E. Sumner, Degradation of a Multilayer Insulation Due to a Seam and a Penetration, TN D-8229, Lewis Research Center, Cleveland, OH, 1976.
- [34] Y. S. Choi, M. N. Barrios, et al., Thermal Conductivity of Powdered Insulations for Cryogenic Storage Vessels, in: *Advances in Cryogenic Engineering*, Vol 51, American Institute of Physics, Melville, NY, 2006.
- [35] W. Boroski, T. Nicol, et al., Thermal Performance of Various Multilayer Insulation Systems Below 80K, Presented at the Fourth Annual IISCC Conference, New Orleans, LA, Fermi National Accelerator Laboratory, Batavia, IL, 1992.

- [36] Robert J. Stochl, Basic Performance of a Multilayer Insulation System Containing 20 to 160 Layers, NASA TN D-7659, National Aeronautics and Space Administration, Washington, D.C., 1974.
- [37] J. P. Sass, C. R. Fortier, Atmospheric Pressure Effects on Cryogenic Storage Tank Boil-Off, in: , Presented at the Cryogenic Engineering Conference, Chattanooga, TN, 2007.
- [38] J. J. Dalton, Evaluation and Modeling of Evacuated Cryogenic Insulations, M.S. Thesis, University of New Hampshire, 2005.
- [39] S. L. Bapat, K. G. Narayankhedkar, et al., Experimental Investigations of Multilayer Insulation, *Cryogenics* 30 August (1990) 711-719.
- [40] P. J. Sun, J. Y. Wu, et al., Experimental Study of the Influence of Degraded Vacuum on Multilayer Insulation Blankets, *Cryogenics* 49 (12) (2009) 719-726.
- [41] T. Ohmori, M. Nakajima, et al., Lightweight Multilayer Insulation to Reduce the Self-Compression of Insulation Films, in: *Advances in Cryogenic Engineering*, Vol. 47B, American Institute of Physics, Melville, NY, 2002, pp. 1565-1572.
- [42] J. E. Fesmire, S. D. Augustynowicz, Method of Testing Thermal Insulation and Associated Test Apparatus, 6742926, 2004.
- [43] J. E. Fesmire, S. D. Augustynowicz, et al., Thermal Performance Testing of Cryogenic Insulation Systems, in: *Thermal Conductivity 29*, DEStech Publications, Lancaster, PA, 2008, pp. 387-396.
- [44] Randall F Barron, *Cryogenic Heat Transfer*, Edwards Brothers, Ann Arbor, MI, 1999.

- [45] A. Hedayat, L. J. Hastings, et al., Analytical Models for Variable Density Multilayer Insulation Used in Cryogenic Storage, in: Advances in Cryogenic Engineering, Vol 47, Plenum Publishers, NY, 2000, pp. 1557-1564.
- [46] W. L. Johnson, S. G. Sutherlin, et al., Mass Optimization of Cryogenic Thermal Insulation Systems for Launch Vehicles, AIAA-2008-7765, American Institute of Aeronautics and Astronautics, Reston, VA, 2008.
- [47] CT-STP-005 Cylindrical Insulation test Aparatus, Rev. A, 2007.
- [48] R. B. Jacobs, Theory of Boil-Off Calorimetry, The Review of Scientific Instruments 35 7 (1964) 828-835.
- [49] J. E. Fesmire, S. D. Augustynowicz, et al., Equipment and Methods for Cryogenic Thermal Insulation Testing, in: Advances in Cryogenic Engineering, Vol. 49, Plenum Press, NY, 2004.
- [50] National Institute of Standards and Technology, Cryogenic Material Properties Polyethylene Terephthalate, NIST Cryogenic Technologies Group Material Properties, Accessed: July 10, 2010, Published: September 4, 2008, http://cryogenics.nist.gov/MPropsMAY/PET/PET_rev.htm.
- [51] S. Dye, A. Kopelove, et al., Integrated and Load Responsive Multilayer Insulation, in: Advances in Cryogenic Engineering, Vol 55B, American Institute of Physics, Melville, NY, 2010, pp. 946-953.
- [52] S. L. Bapat, K. G. Narayankhedkar, et al., Performance Prediction of Multilayer Insulation, Cryogenics 30 August (1990) 700-710.

- [53] Lixing Gu, Generalized Equation for Thermal Conductivity of MLI at Temperatures From 20K to 300K, in: , ASME Conf. Proc. 2003, 467, 2003.
- [54] R. J. Corruccini, Gaseous Heat Conduction at Low Pressures and Temperatures, Vacuum II & III (1959) 19-29.